Effect of Coil Configuration on Dynamic Wireless Power Transfer for Electric Vehicle Applications

Research Thesis for M.Sc. Degree

By Sahar Bareli

Supervisors – Prof. Yosef Yeshurun
– Dr. Shuki Wolfus

Institute of superconductivity and magnetic measurements,

Bar-Ilan University, Israel

26/09/2021

Acknowledgements

The work was funded in part by the Israeli Ministry of Environmental Protection.

I thank a scholarship received from the Israeli Smart Transportation Research Center (ISTRC).

I would also like to thank O. Ezer and H. Rumbak from “Electreon Ltd.” for useful discussions and information shared with us.

Finally, I personally and sincerely thank Prof. Yosef Yeshurun and Dr. Shuki Wolfus for their wonderful and insightful supervision, for their professionalism, kindness, and support throughout my entire M.Sc.

Contents:

1. *Abstract*

Dynamic Wireless Power Transfer (DWPT) technology enables the process of charging the on-board battery of an Electric Vehicle (EV) while on the move and along its travel path, eliminating the need to stop for charging. Inductive coupling between the receiver and transmitter systems is used to transmit energy from transmitting coils embedded in the road to receiving coils attached to the EV chassis. The dynamic nature of the energy transfer allows the on-board battery to be minimized in dimensions, capacity and weight. This reduced EV battery leads to dramatic energy savings due to the reduced vehicle weight, as well as to significant environmental advantages, caused by minimizing CO_2 emissions during production, and to reduced hazardous waste and contaminants during disposal.

This research focuses on the energy transfer process between the transmitting and receiving coils aiming at improving the efficiency of this energy transfer and advancing DWPT technology to a level which supports large scale implementation in the near future of smart transportation. To achieve this goal, we have studied the electromagnetic coupling between the transmitter and receiver arrays as we explore various layout configurations. Variations to the coil dimensions were made as well as changes to other geometry parameters and use of magnetic materials. This study first explores cases where the DWPT configuration is stationary namely, the electromagnetic interaction is explored while all geometry and distance parameters are fixed. We then switch to the dynamic scenario namely, when the system is in motion and the distance between the coils changes and/or when misalignments occur, mimicking realistic scenarios.

The study has been performed using Finite Element Method electromagnetic simulations tool. By optimizing the DWPT design we managed to improve the energy transfer to the EV. We demonstrated that by understanding and controlling the spatial magnetic field distribution generated the transmitter coils, it is possible to design a receiver coil array which picks-up maximal magnetic flux. Such maximum is obtained for each receiver coil dimension at the point in space where the perpendicular magnetic field component generated by the transmitter reverses its

direction. We have shown that in a stationary scenario, under such conditions, it is possible to achieve energy transfer efficiency higher than 92%! This is to be compared with the less than 80% efficiency of the coils layout prior to our optimization. A similar improvement is expected for EV in motion. We have also revealed a new phenomenon for EV in motion, namely that the coupling coefficient varies with the relative movement between the coils and, as a result, the self-resonance frequency of the system splits to two separated frequencies. This split, observed here for the first time, depends on the coupling strength, increasing with its increase. It is expected that this split will affect the design of DWPT systems and therefore must be taken into consideration in any future designs.

In addition, we have investigated the non-ionizing radiation levels in a typical DWPT layout. Simulations of scenarios which include ferromagnetic screening allowed us to improve the design and reduce the radiation from the transmitting coils and the conducting cables. We managed to reduce the radiation to levels significantly lower than worldwide recommendations.

The study described here offers new ways for optimization of DWPT systems with improved energy transfer efficiency. Such optimization translates into direct energy savings and smaller batteries, thereby to economic savings and reduced CO_2 emissions.

We are convinced that the findings of this work may be used to improve current DWPT designs, and, in turn, create safer, greener, and more efficient use of the technology.

2. Introduction

The introduction is organized as follows: Sub-section 2.1 gives a broad background of the world of EVs, WPT, and DWPT. In the following two sub-sections, (2.2 and 2.3), we explain the mechanisms governing inductive power transfer and resonance power transfer. Subsection 2.4 gives a brief explanation to how DWPT operates. Finally, in subsections 2.5 and 2.6, we describe some types of commonly used receiver and transmitter coils configurations in DWPT systems.

2.1. Background

The world of electric vehicles (EVs) is a vast and fascinating one. These vehicles have the potential to revolutionize the way we view and use transportation today. They promise a cleaner, greener alternative to the classic, outdated, environmentally hazardous combustion engine used in most vehicles since the dawn of the last century. Instead of using polluting "power plant" inside of every vehicle, EVs can use the electric power that is generated elsewhere (including using greener methods such as solar panels and wind turbines), drastically reducing the pollution concentration in urban places and busy roads. EVs are also more efficient, as the power is generated in an efficient power plant instead of an inefficient combustion engine. They are also far more quiet than normal vehicles, as they run on batteries, which can potentially reduce drastically the noise pollution in busy urban areas. Finally, the inclusion of a battery as the power source indicates a fully electronics-based vehicle, which is easy to integrate into a data collection system, making data collection far more efficient. Overall, EVs offer a clear upgrade to everyone's quality of life.

While EVs are considered the vehicle of the future, the solution offered by 'traditional' EVs, driven by batteries which are charged frequently in fixed location, is still facing many challenges that need be addressed. EVs still provide a challenge to the environment and to the energy eco-system. In particular, batteries are large and heavy to allow for long-distance travels and are, because of their size, a serious environmental hazard. In addition, the large battery size results in large CO_2 emissions during the production process of the batteries, using non-renewable materials like lithium, and result in a vast amount of toxic waste once the battery inevitably depletes [1,2]. Batteries are not only hazardous, but they also dramatically increase the mass of the EV; in some cases, batteries can weigh up to half of the EV's total weight. Such heavy load being carried along with the EV greatly impacts the energy efficiency of the vehicle, while also being a big cause for expensive and potentially dangerous recalls, as was done by numerous big vehicle companies in recent years [3]. Another pressing issue with current electric vehicles is that its charging process is slow and cumbersome compared to the combustion engine alternative. Nobody is willing to wait for refueling/charging more than a few minutes and fast battery charging has yet a long way to advance to reach this milestone. Furthermore, the current infrastructure of charging stations is severely lagging behind the gas alternative [4], making it almost impossible to take an EV into a long journeys. Finally, as EV charging is typically done in certain times of the day (night-time for example) and requires a large amount of electricity [5,6], the electrical grids of heavily populated urban areas may not be able to support such heavy load, making EV charging practically impossible when their number increases.

Wireless power transfer (WPT) technology introduced a new way of charging EVs in a more convenient manner. While WPT indeed makes the charging of EVs easier and more comfortable for the user (for example, while parking on a designated spot), it does not address most of the fundamental issues mentioned above.

A breakthrough solution is provided by the Dynamic Wireless Power Transfer (DWPT) technology that enables the charging of the EV 'on the go', thus significantly reducing the on-board battery size and weight. In principle, dynamic charging will enable unlimited driving range and the on-board battery is required just to allow short off-course deviations for recharging. This results in an increased energy efficiency for the EV, both in terms of energy usage and production. Since batteries are far smaller in DWPT, CO_2 emissions and hazardous waste are greatly reduced during production and on battery's end of life [7]. Charging station infrastructure is simply unnecessary for DWPT, as the vehicle is charged during drive, meaning that the load of the electric grid is spread throughout the day, making it far easier to implement in urban environments. The small battery allows for some deviations from the charging route, meaning the EV is not bound to a track, while also having a potentially unlimited range. Since all EVs that use DWPT are using these roads together, energy sharing between vehicles can also be implemented for further efficiency increases. Finally, such a system will be even easier to integrate into big data collections, as the roads themselves can be used to record data of traffic, battery life, battery usage *etc.*, which can be used for Artificial Intelligence studies and central planning and control.

While this all sounds well and good, many new questions and issues arise when moving from cable charging to WPT, and even more complex problems arise when moving from WPT to DWPT. Arguably, one of the most important questions is safety – can we be sure that the non-ionizing radiation that this system emits is safe? What are the non-ionizing radiation levels that reach the passengers? Another important question is the question of the energy transfer itself. Mid-field power transfer is much harder to implement than wired power transfer, as the energy transferred is heavily reduced with distance. In the case of WPT this can be fixed by a retractable receiver coil that is lowered while parking, however this is impossible to implement during drive due to regulations which dictate the allowed clearance between the road and the vehicle chassis. Furthermore, in the case of DWPT, the coupling between the transmitting road embedded system (transmitter coils), and the energy receiving system (receiver coils) that is attached to the chassis of the EV is subject to extreme changes during the drive and must be addressed. Other open questions that need be explored are how expensive is this system to implement? Can the electric grid support dynamic charge on a large scale? Is it possible to implement such a drastic infrastructure and behavioral change on a global scale?

This work aims to answer the first two questions presented above: The question of radiation, and the question of mid-field energy transfer and efficiency. Both questions are analyzed and answered utilizing electromagnetic simulations which shed light on the processes governing DWPT mechanisms and allow us to propose improved designs for reaching better energy transfer and safer operation

2.2. Inductive Power Transfer

The term “inductive power transfer” refers to the process of transferring energy between inductors with no physical contact between them (wirelessly). It is the main method in use today for short range wireless power transfer (WPT) [8].According to Ampere's law, current in a coil produces a magnetic field B in space described by:

$$\nabla \times B = \mu_0 J$$

This equation implies that a current flowing in a conductor creates a magnetic flux field, and vise-versa. With this in mind, one can transfer energy from one system to another using coils: an AC current flows through a transmitter coil, which creates an oscillating magnetic field. This field passes in part through a receiving coil, which in turn induces an alternating voltage in accordance with Faraday's law of inductance:

$$\nabla \times E = -\frac{\partial B}{\partial t}$$

This induced voltage may then be used to drive a load.

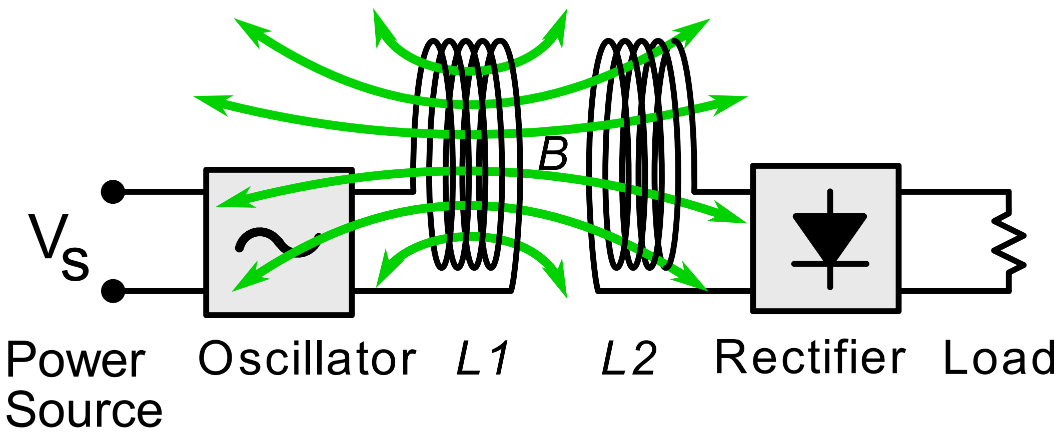

Figure 1: Inductive Power Transfer. The transmitter coil L_1 is connected to an oscillator. Some of the magnetic flux is then picked up by the receiver coil L_2, which is connected to the load [9].

Figure 1 displays schematically a typical 2-coils scenario. The coil L1, fed by an oscillating voltage source, is the transmitting coil. The receiving coil L2 is mounted apart at some distance and is connected to the load through a rectifying circuit element. Marked by the green arrows, are the magnetic field lines generated in L1 and partially crossing through L2. As seen clearly, some field lines would close in space without interacting with L2, hence the coupling between the coils is not perfect. The amount of coupled magnetic flux between the coils is described by the mutual inductance of the transmitter and receiver coils, defined as:

$$L_{1,2} = V_2 / \frac{dI_1}{dt}$$

where I_1 is the current flowing in the transmitter coils, and V_2 is the induced voltage across the receiver. The mutual inductance of the coils can be used to define the electromagnetic coupling coefficient, k, between the transmitters and receivers. k, then, represents the fraction of transmitter induced flux that is 'absorbed' by the receiver:

$$k = \frac{L_{1,2}}{\sqrt{L_1 L_2}}$$

where L_1, L_2 are the self-inductances of the transmitter and receiver coils respectively. The voltage in each circuit is, therefore:

$$V_1 = i\omega L_1 I_1 + i\omega L_{1,2} I_2$$

$$V_2 = i\omega L_{1,2} I_1 + i\omega L_2 I_2$$

Classic inductance coupling is effective in near-field applications, as the energy transfer is completely dependent on the distance between the two coils, and therefore is severely reduced with distance. Therefore, it can only be used for applications such as transformers, small appliance chargers *etc.,* where k is roughly close to 1. However, it is extremely inefficient for far-field applications. Specifically, for Electric Vehicle (EV) charging, due to the relatively large air gap between the chassis of the vehicle and the road (about 30 cm), it is necessary to enhance the inductive coupling. This mid-range distance is especially problematic, as the mutual inductance is rather weak, and k is of the order of 10%. It is impossible to effectively charge an EV with such poor transfer rates. In order to achieve sufficient power transfer at these ranges, one must use magnetic resonance coupling.

2.3. Magnetic Resonance Coupling

To overcome the unique challenges of low k, mid-range, wireless power transfer, Magnetic Resonance Coupling [10] becomes a must, in particular for EV charging. This technique takes full advantage of resonance theory. One can look at the swing analog to get an idea of the principle of operation of the magnetic resonance coupling. If one was to gently push a swing at exactly the right frequency, i.e., the self-resonance of the swing, even though the kinetic energy of the swing was acquired in very small increments, it will quickly grow in magnitude. The same goes for the case of magnetic resonance coupling – instead of transferring the energy with 'brute force', we transfer small "packets" of energy at the resonant frequency of a tunable electric circuit connected to the receivers, which allows for orders of magnitude higher energies to be transferred wirelessly. Implementing resonance coupling to WPT, power is still transferred inductively, however both transmitter and receiver coils are separately connected to a respective resonator circuit. If both resonators share the same resonance frequency, power can be transferred far more efficiently and through larger air gaps. The impedance of a simple RLC series circuit is given by:

$$Z(i\omega) = R + i(X_L - X_C)$$

$$X_L = \omega L$$

$$X_c = \frac{1}{\omega C}$$

It is easy to see that at $X_L = X_C$ we get a minimal impedance, resulting in minimal AC resistance. Operating at this resonance frequency, the reactive energy oscillates between the coil and the capacitor and is built up with each cycle of the source. As part of the energy is still lost in the circuit resistance, one must also consider the quality factor, Q, of both transmitter and receiver circuits. Q is defined to be the energy stored in the circuit over the energy dissipated by the impedance of the circuit. For the above discussed series resonator:

$$Q = \frac{\omega_0 L}{R} = \frac{1}{R\omega_0 C}$$

Using these parameters, we can represent the impedance of a series resonator as

$$Z = \sqrt{\frac{L}{C}}\left(i\left(\frac{\omega}{\omega_0} - \frac{\omega_0}{\omega}\right) + \frac{1}{Q}\right)$$

Using these definitions, we can deduce that for a series resonator, operating at its self-resonance frequency, the induced voltage as function of the source voltage is:

$$V_0 = \frac{iX_L}{R} V_{in} = iQV_{in}$$

With Q typically in the range of a few hundred for WPT applications, this implies that with resonance coupling, the induced voltage on the receiver system is orders of magnitude higher than in inductive power transfer (IPT) if not under resonance operating conditions.

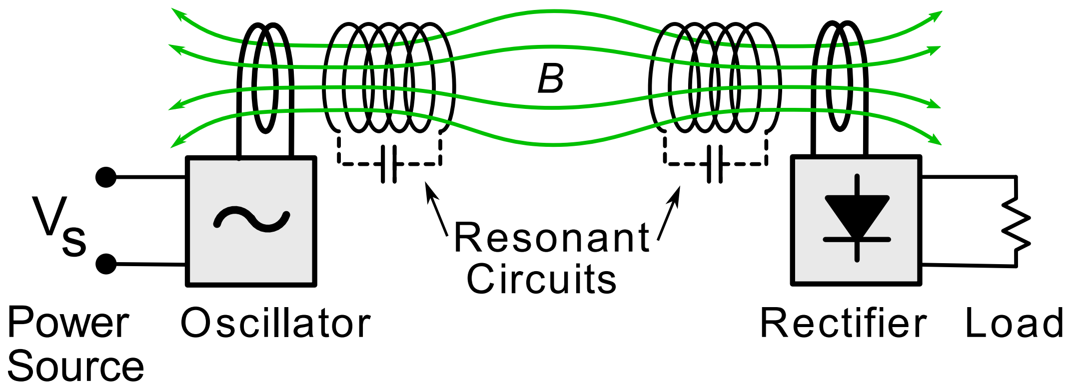

Figure 2: Resonant inductive power transfer. Both transmitter and receiver coils are connected to a resonator, meaning the power transferred between them is vastly increased [9,11].

Consider the loosely coupled resonators seen in figure 2, with the same resonance frequency ω_0, the voltage equations of such a system are (assuming zero load):

$$V_1 = \left(R_1 + i(X_L - X_C)\right)I_1 + i\omega L_{1,2} I_2$$

$$0 = i\omega L_{1,2} I_1 + \left(R_2 + i(X_L - X_C)\right)I_2$$

In the separated coils scenario of Figure 2, the coupling between the two circuits is relatively weak because of the distance between the coils. We can thus assume that the mutual inductance $L_{1,2}$ is small, and that the back-effect of the secondary circuit on the primary is small in comparison with its primary current. Therefore, we may neglect the $i\omega L_{1,2}I_2$ term in the first equation. At resonance, we obtain that:

$$I_1 = \frac{V_1}{R_1}$$

Therefore, we can solve for the second equation and obtain the induced current:

$$I_2 = -\frac{i\omega L_{1,2}V_1}{R_1R_2}$$

The power dissipated on R_1 and R_2 is therefore given by:

$$P_1 = \frac{V_1^2}{2R_1}$$

$$P_2 = \frac{V_1^2R_2\omega^2L_{1,2}^2}{2(R_1R_2)^2}$$

Finally, we can calculate the power transfer between loosely coupled resonators using magnetic resonance coupling:

$$\frac{P_2}{P_1} = \frac{\omega^2L_{1,2}^2}{R_1R_2} = \frac{\omega^2k^2L_1L_2}{R_1R_2} = k^2Q_1Q_2$$

This means that the power transfer between two circuits at mid-field is strongly tied to the coupling coefficient k^2, as in WPT without resonance. However, when implementing resonance operating conditions, the power transferred is also multiplied by the Q-factors of both circuits. Therefore, one's target is to increase both k and Q_1, Q_2 to significantly improve the energy transfer efficiency of the system. In this work we explore also the resonance conditions for various coils scenarios but mainly focus on ways to significantly improve the coupling between the primary and secondary circuits.

2.4. Dynamic Wireless Power Transfer

In the world of transportation, the holy grail is reaching a state where vehicles are not required to stop for fueling/charging. This would support unlimited travel time and range, and a non-stop service in public transportation. As fictional as this idea sounds, one technology may assist to realize and materialize this concept. This is the Dynamic Wireless Power Transfer technology, which has been rising in popularity in the past decade [10,12–20]. Applying the same energy transfer methods on a moving system, one can, in theory, achieve operational dynamic charge for EVs to support the coveted unlimited travel range/time. Many factors are to be considered when designing a functional DWPT configuration as there is a vast number of changing variables and challenges that need to be addressed during the simplest of drive segments. The present research work tackles some of these issues, in particular changes in the coupling coefficient during motion, track and EV misalignments, and position-dependent resonance frequency, all affecting the energy transfer efficiency of the DWPT system. With that in mind, various configurations have been tested over the years. To demonstrate the various approaches, we focus here on the two largest projects currently in development in the world: the South Korean online electric vehicle (OLEV) project [21], and the demonstration projects run by the Israeli company Electreon in Sweden and Israel [22]. Both projects have demonstrated time and again how effective and realistic DWPT can be. The South Korean OLEV project was the first large project in the world to utilize the concepts of DWPT and created the first dynamically charged bus. An example of a bus that is charged wirelessly can be seen in figure 3. Transmitter coils are embedded in the road, and receiver coils are placed at the chassis of the bus. The successful Electreon Swedish road prototype has garnered vast interest and promise for the future of DWPT, as they managed to fully electrify about 1.5 km of road and successfully charged an electric truck [23]. The project showed the viability of DWPT systems and their rather simple implementation, while also integrating a state-of-the-art communication system which provides real-time communication with each vehicle that utilizes their system. That being said, much work is still needed to fully utilize this technology and make it as energy efficient as possible. The following section will go over major configuration topologies for both transmitting and receiving systems.

Figure 3: OLEV track, South Korea [24]*. The OLEV bus drives on a power track that transmits electric flux during the drive. The cyan lines represent the optimal travel route that promises optimal energy transfer and charge. The receiver coils are mounted below the chassis of the bus, which receives the transmitted energy from the road and transfers it to the on-board battery.*

2.5. Transmitter Configurations

A typical layout for a dynamic wireless power transfer setup consists of the following major components: power supply, transmitter circuit, receiver circuit, load, and, of course, the space surrounding the array which includes materials that may influence the process. We begin our study by focusing on the transmitter coils configuration.

Various transmitter configurations have been tested in the past, mostly as part of the Korean OLEV project [12,14,24] mentioned above (figure 3), who were the first to revolutionize WPT and produced a working prototype of a functional DWPT system, by implementing recharging road segments into Korean roads. It was first launched during March 2010 and was developed and operated by The Korea Advanced Institute of Science and Technology (KAIST).

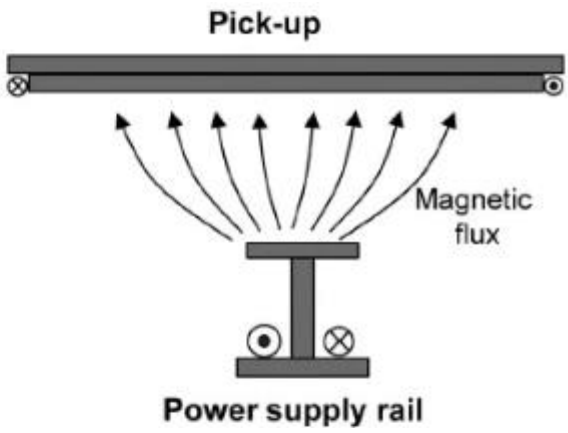

Figure 4: I-type transmitter configuration. The transmitter coil is wrapped around an I-shaped magnetic core, which helps to increase flux transfer by directing it upwards [25].

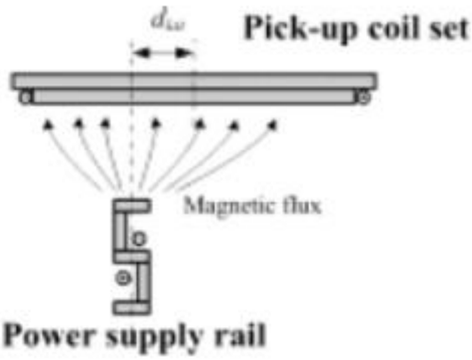

Figure 5: S-type transmitter configuration. The transmitter coil is wrapped around a S-shaped magnetic core instead, increasing the effective range of power transfer [26]. *This configuration is superior due to the core's shape being more central, which in turn directs the flux lines more effectively into the receiver coils.*

The first OLEV project utilized an "I-type" module (figure 4) [25] used to direct the flux lines from the transmitter into the receiver coils. This, however, offered a good spatial magnetic flux coverage at a somewhat limited range. They later changed the I-type module into an S-type one (figure 5), which included an S-shaped power supply rail for better transmitter range [26]. This improved upon its predecessor by effectively doubling the distance that the receiver coils and the transmitter coils can be placed while also reducing EMF well below non-ionizing radiation guidelines [27].

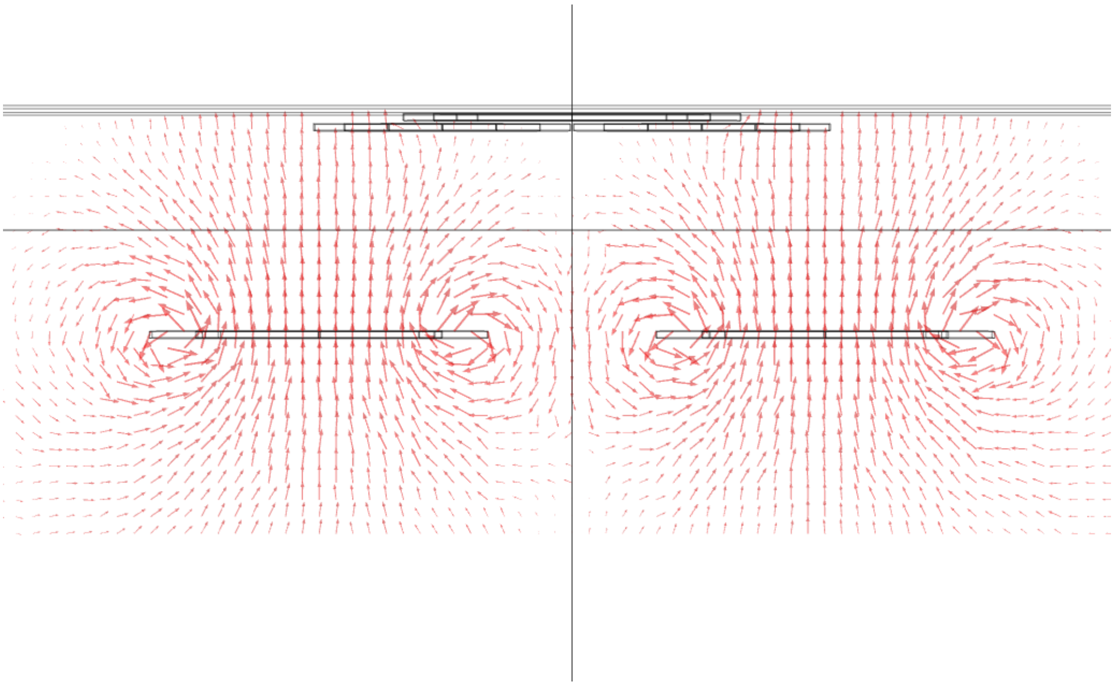

Figure 6: An example of the flux lines of a unipolar configuration, simulated by us. Each transmitter coil has a counterclockwise current applied to it. This results in spatial gaps in the flux field.

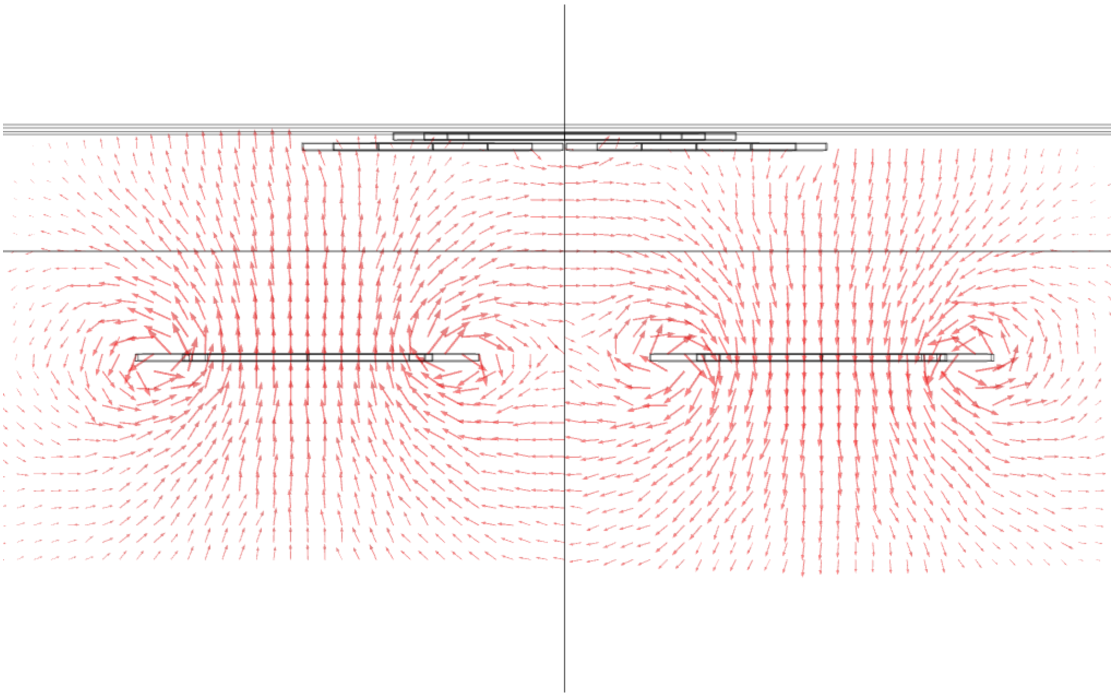

Figure 7: An example of the flux lines of a bipolar configuration, simulated by us. Each transmitter pair is applied a clockwise and counterclockwise current in a 'figure of eight' manner, resulting in an alternating positive-negative field. This method is preferred since it has less flux gaps in-between the coils.

Unipolar and bipolar coils were also tested during the Korean OLEV project [8,28,29]. We have simulated examples of unipolar and bipolar coils and the spatial magnetic field distribution is presented in figures 6 and 7 respectively. Unipolar coils operate under the principle that all coils have currents flowing in the same direction, resulting in a more direction-oriented flux field. While the unipolar coils are much easier to implement, as they require simple geometries, they are outperformed by their bipolar counterparts, since a bipolar configuration confines the flux lines into a more specific region under the receiver coils. The magnetic flux distribution over the bipolar transmission coils becomes more uniform in general, as the flux no longer cancels with itself at the seams. As apparent in figure 6 (the unipolar case), this configuration results in a drop in the magnetic flux intensity around the middle, between the coils which means that the field is less uniform in nature. This in turn means that some areas do not receive any flux in them at all, namely, that the EV is not receiving energy during the pass over this space segment. This can be mitigated in a static case by placing the receiver coils in the optimal location, however in a dynamic case this can result in poorer energy transfer efficiency. In figure 7 we show our simulation results for the bipolar case. Apparently, in this case, the flux distribution is much more uniform. The bipolar configuration also increases the coupling coefficient and reduces residual EM radiation. Our results will be further described later in this dissertation.

2.6. Receiver Configurations

Turning next to the receiver coils configuration, variations of coil layouts, number of coils and coil geometry have been explored in the past, with varying levels of efficiency.

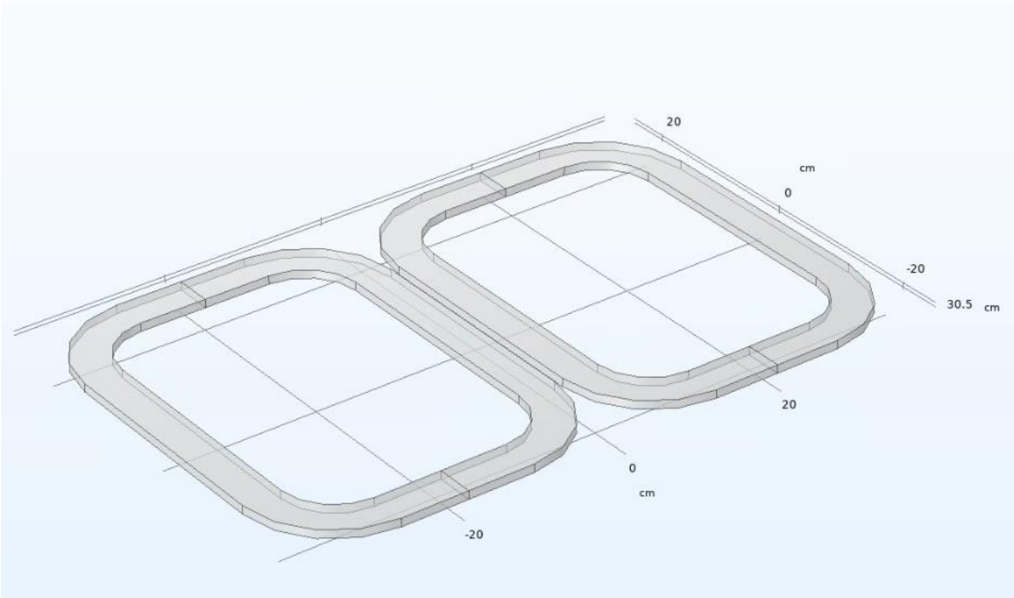

Figure 8: Simulated 'DD' configuration of the receiver coils placed under the chassis of the EV.

One of the most effective receiver bipolar configurations is the "double-D" (DD) shape configuration, where two rectangular coils are laid side by side to form a "double-window"-like shape, described schematically in figure 8. The two 'D' coils are connected in opposite directions to pick the net sum of two opposing signs magnetic field lines. Still, the DD configuration is very susceptible to position variations. Clearly, when the EV travels along the transmitter coils track, large variations in the picked-up flux occur, including a point of minimal signal, where the DD layout is positioned above one of the transmitter coils. An example of a simulation of the energy transfer in a 'DD' configuration is displayed in figure 9. It describes the changes to the coupling coefficient to an EV along a travel path. The red circle represents the fully aligned case where the EV is directly above the transmitters, and the green rectangle represents a misaligned case where the EV continued past the transmitters. Since k is the more fundamental parameter which affects transfer efficiency, as it represents the strength of the coupling between the transmitter and receiver coils, it will be regarded as the parameter of choice in our simulations. The coupling coefficient sharply declines at two locations during movement, effectively creating two 'dead' zones were the flux picked up by the receiver coils practically zeroes. It is therefore easy to see that such configuration can work for static purposes only, as the maximal flux collection occurs exactly when the centers of the receiver and transmitter coils overlap.

A step forward is the double-D quadrature (DDQ) configuration [16], which includes an additional single coil mounted at the center and on top of the DD layout (figure 10). It provides a good solution to DWPT, since it can pick up increased amounts of magnetic flux lines relative to its similar in size, DD configuration. It is also far less susceptible to misalignments, as the square Q-shaped coil covers the 'dead' zones of the DD coils, effectively increasing the flux pickup. This can be seen in figure 11, which describes the changes to the coupling coefficient k as a function of transmitter-receiver relative shift along the travel path. Each line represents k for one of the three coils in the DDQ configuration.

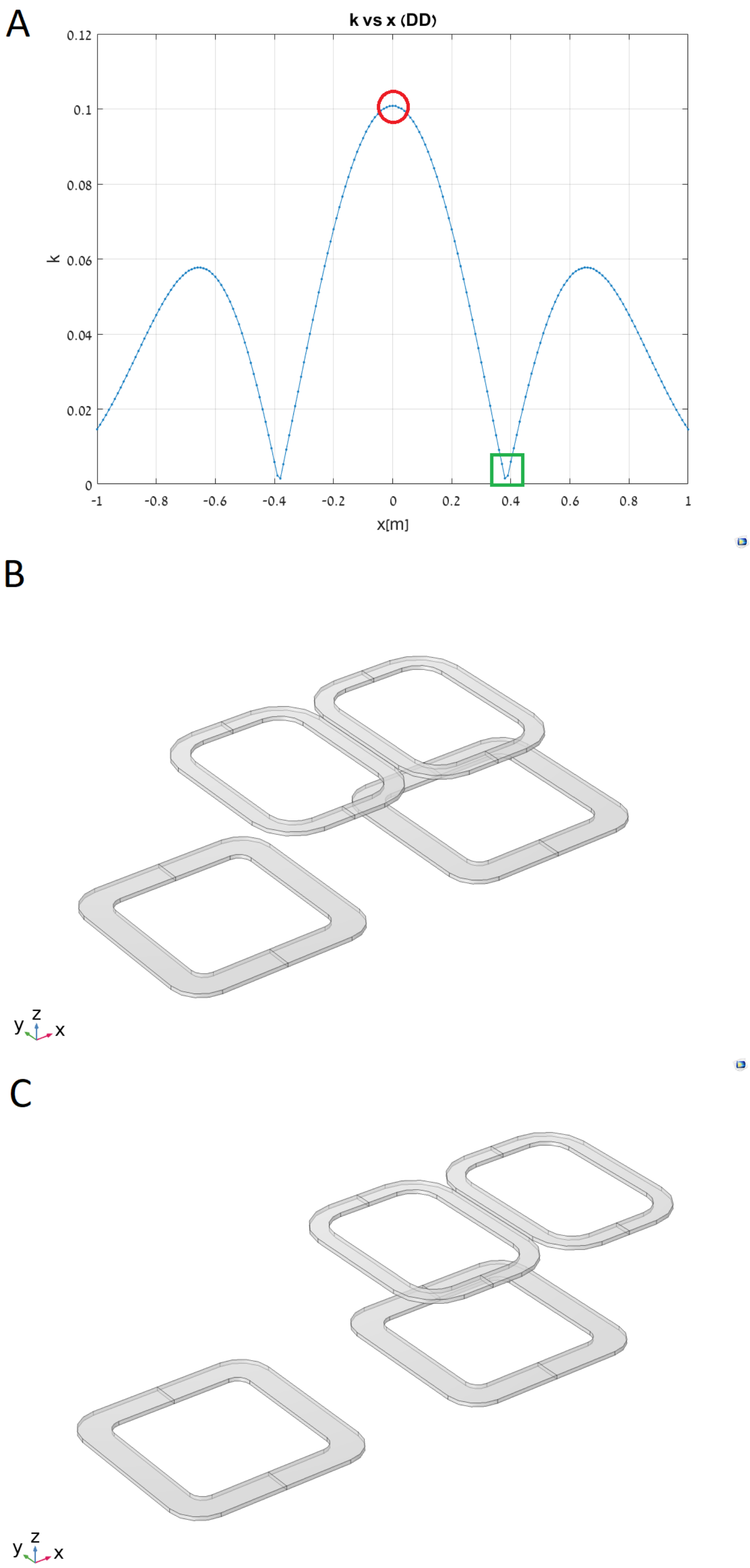

Figure 9: 'DD' configuration shift effects. A: Changes to k as a function of misalignments along the travel path. The red circle represents the configuration shown in B, and the green rectangle represents the configuration shown in C. In both cases, the receivers

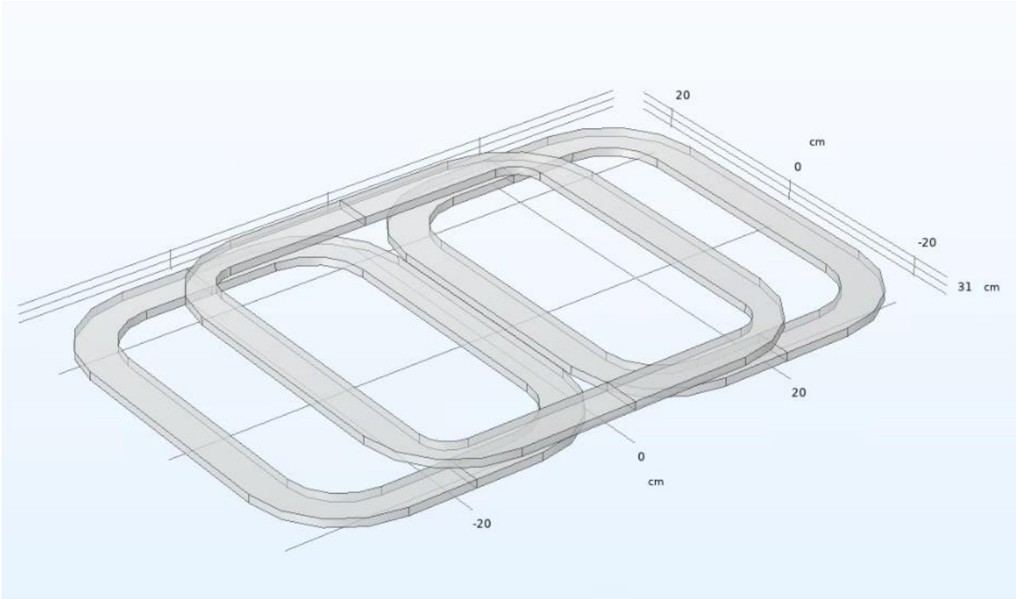

Figure 10: Simulated 'DDQ' Configuration of the receiver coils placed under the chassis of the EV.

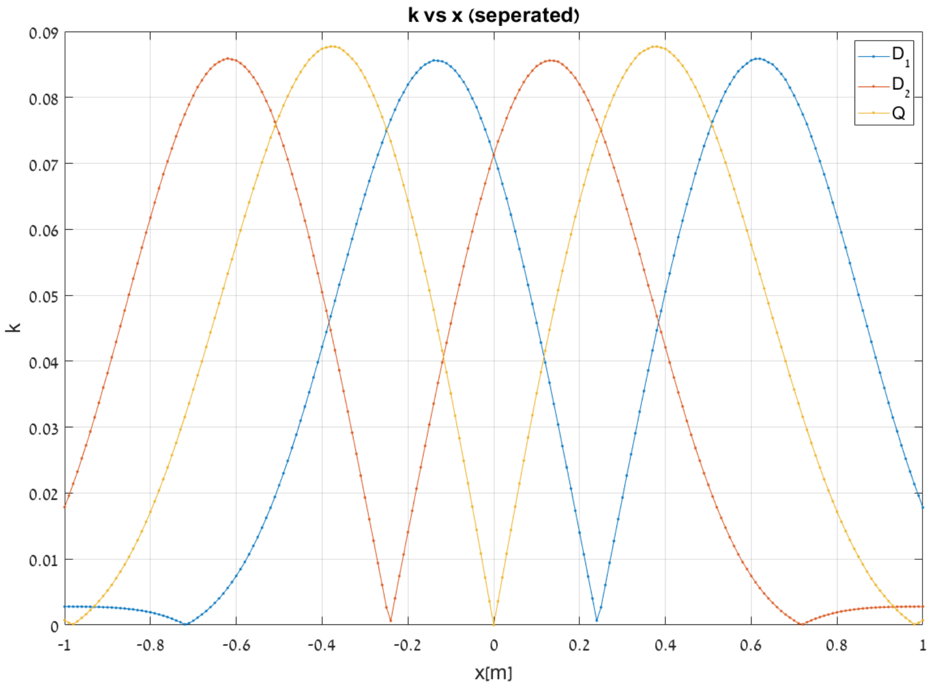

Figure 11: 'DDQ' configuration coupling coefficient as a function of travel path misalignment. Each coil effectively 'covers' for the 'dead zones' of the other coils, creating a sort of diode-bridge type of configuration.

The focal point of this work is the exploration of improvements to the energy transfer system by varying the receiver and transmitter coils. In addition, non-ionizing radiation, and the screening of said radiation was explored. The study of the position dependent electromagnetic energy transfer has also produced interesting results that show a splitting of the resonance frequency of the system as a function of the coupling coefficient k. The results, to be described below in detail are extremely important for designing improved, highly efficient DWPT systems.

The rest of the work is organized as follows: After describing the research goals (chapter 3), we discuss the physics behind the COMSOL Multiphysics simulation tool, our main analysis tool (chapter 4). We then move to a detailed description of our results, starting with results for a stationary vehicle (chapter 5.1 and 5.2) and then to a moving vehicle (5.3). In chapter 5.4 we introduce, for the first time, a phenomenon of double resonance in a moving car. Summary of our main findings and our conclusions are presented in chapter 6.

3. Research Goals

DWPT technology is still in its infancy and requires further research and optimizations to be operational. This work tackles some of the issues currently in the front of DWPT research and development. As we explore better and improved configurations and layouts, we aim at gaining better understandings about the physics that governs energy transfer in DWPT systems. As we acquire more insight into the electromagnetic field distribution and interactions, we expect to be able to provide answers to the main question in this field: how can WPT and DWPT technologies be significantly improved to make them feasible for real life use? What are the limits for energy transfer in such wireless charging technologies? Will they be capable of competing with state-of-the art traditional charging methods? These questions are more complex than one might think on first glance, as there are many variables that must be taken into consideration. In this work, we have isolated the effect of such parameters by utilizing simulation tools. Varying one parameter at a time while keeping the other fixed allowed us to reach a better understanding. For example, after varying the longitudinal aspect of the “DD” receiver coil dimension, we have identified the location where the direction of magnetic field generated by the transmitter coils reverses directions and starts to contribute negatively to the picked-up flux. In a similar manner, we’ve separated the contributions of the transmitter coil dimensions, misalignments, coupling coefficient and resonance frequency to the energy transfer. We will describe these results right after the Methods chapter.

4. *Methods*

The main tool used in our study is numerical simulation. This is to replace a real-life measurement system since every small change to the configuration is extremely expensive and slow to produce, which will make the whole work impossible. Specifically, all simulations presented in this work were simulated using COMSOL Multiphysics simulation tool [30]. It uses finite element method (FEM) to numerically solve physics-based systems of partial differential equations (PDEs) [31]. It is one of the most common and efficient modern methods used in both physics and engineering and is extremely effective in solving linear and non-linear physical systems.

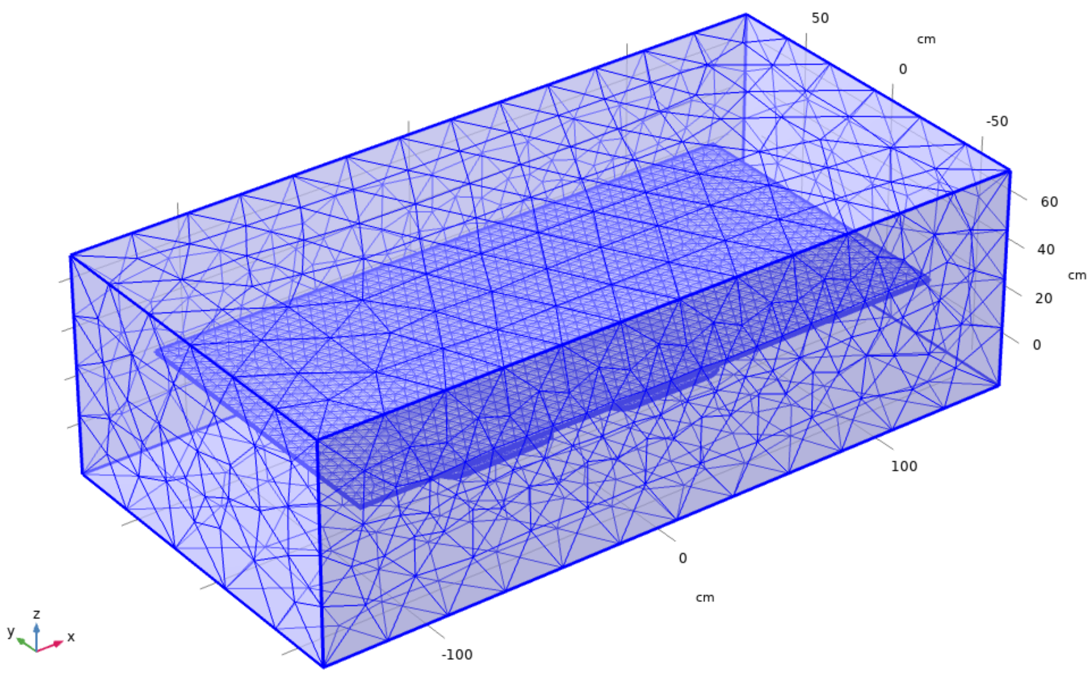

Figure 12: Mesh example for the simulated DWPT system. The outer block describes the 'world' in which the system lives in. It is simulated to be air. Inside this block, the receiver and transmitter coils are simulated, as well as the ferrite plate (flat rectangle inside the block). This link system is then converted into an adjacency matrix.

The main idea of FEM is to discretize space using a network of elements called "mesh" (Figure 12), which divides the space into a collection of subdomains. The outer box defines the 'world' for which the system is defined. Inside the box, the coils and a ferrite plate are simulated. Each element is assigned certain properties (for example – material properties such as electric conductance, permeability etc.) and is solved locally using the assigned set of PDEs. Finally, COMSOL recombines the elements using a matrix representation of the mesh to indicate each element and its nearest neighbors and solves for it using known solution techniques called 'solvers'. This tool is very powerful and gives accurate results for complex, real-life systems that are impossible to account for using analytic tools. All simulations were solved using the AC/DC module for COMSOL, specifically using the magnetic field (mf) formulation, which solves the following set of equations in the frequency domain:

$$\nabla \times H = J$$

$$B = \nabla \times A$$

$$J = \sigma E + i\omega D + J_e$$

$$E = -i\omega A$$

These equations solve for the magnetic vector potential A. The frequency domain was chosen over the time domain since the time which takes for the vehicle to pass over the coils is negligible compared to the frequency of the magnetic field generated by the transmitter coils. Working in the frequency domain drastically improves solving time in this case. The electric circuit (ec) formulation was also used for some of the simulations, to couple the geometry to a system of electric circuits.

5. Results

5.1. Static (stationary) Results

5.1.1. Initial Configuration

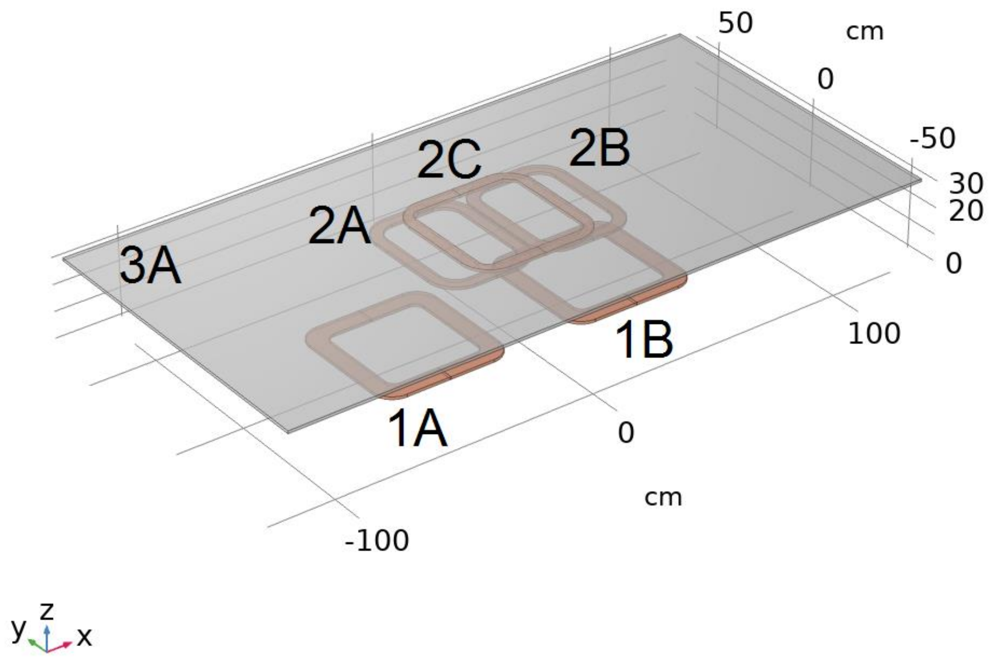

Figure 13: Initial layout of the simulated coil array. 1A, 1B: transmitter coils. 2A, 2B: DD receiver coils. 2C: Q shaped receiver coil on top of the DD receiver coils. 3A: Ferromagnetic ferrite plate.

We begin our study with the DDQ configuration depicted in figure 13. The specific starting point layout and its parameters were given to us as a courtesy from "Electreon", which uses a similar configuration in its pilot projects. Each transmitter coil consists of 11 turns, while the receiver coils have 3.5 turns each. The transmitter coils also form a DD configuration and are placed 25 cm apart. The transmitter 'DD' coils are connected in series in a "figure of eight" manner, such that the current in one coil flows clockwise, while the current in the second coil flows counterclockwise. As previously described, the receiver coils are connected in a similar manner, so that flux in opposite directions crossing each ‘D’ coil is integrated and contribute to the induced voltage.

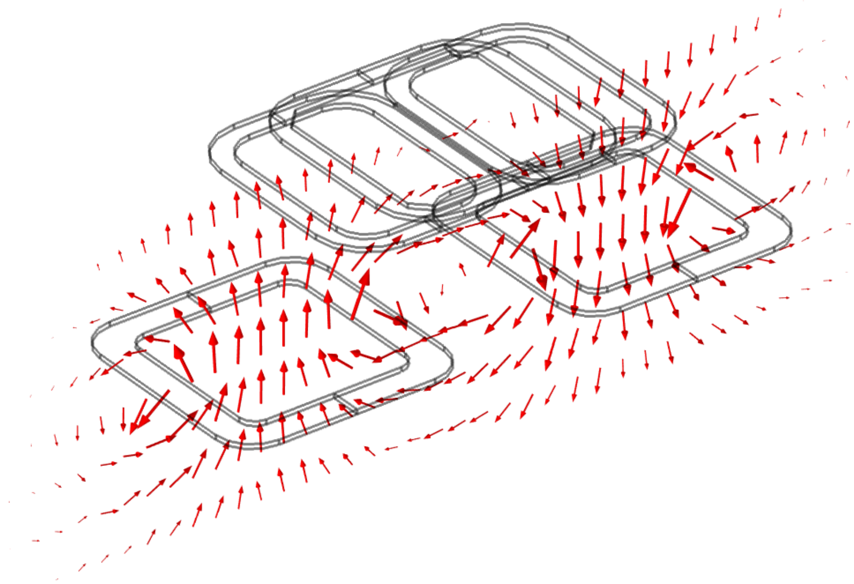

Figure 14: Flux lines generated in the bipolar transmitter coils. The lines are picked up by the ‘DDQ’ receivers.

The transmitter coils, therefore, create a bipolar flux spatial distribution as seen in figure 14, where the flux which enters one coil exits through the other. In all simulations for the transmitter coils, a 50 A RMS, 85 kHz sinewave current was generated, using frequency domain simulation. On top of the receiver coil array, not shown in the figure, a ferrite plate has been placed. This ferrite plate serves to divert flux lines into the receiver coils, as well as a magnetic shield for reducing electromagnetic non-ionizing radiation level at passengers’ level to well below the allowed standards [27]. All non-ionizing radiation concerns will be explored in a later chapter.

5.1.2. Coil Dimension Changes

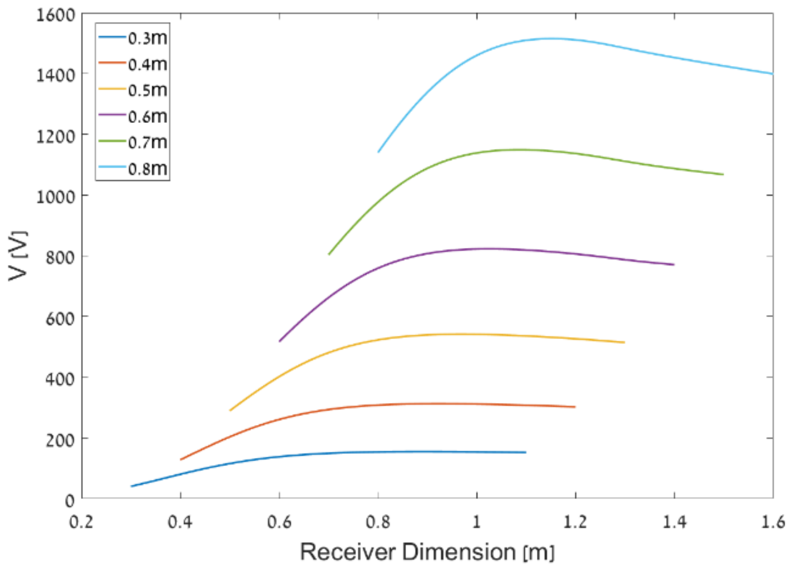

Figure 15: Voltage across receiver as a function of the change in DD coil dimensions. Different curves represent different transmitter coil dimensions from 0.3 to 0.8 m.

Variations to the receiver and transmitter coil dimensions have been made, specifically stretching the “radius” of the DD coils to cover more of the EV’s length and/or width, yielding more effective rectangular shapes. These changes were made with the goal of collecting more flux lines at the receiving coils and were proven to be very successful. In each simulation step, both length and width of the receiver coils were either stretched or compressed by the same value, yielding a Q-shaped geometry in each step. These simulations were repeated multiple times, each time with a different transmitter coils diameter, the results of which can be seen in figure 15. The figure exhibits the voltage induced in the receiver coils as it increases with the increase in transmitter coil size. Also, for each transmitter size, the curve is non-monotonic and there is a corresponding receiver size that receives maximal voltage. Further increase in receiver coil size results in a decrease in the induced voltage.

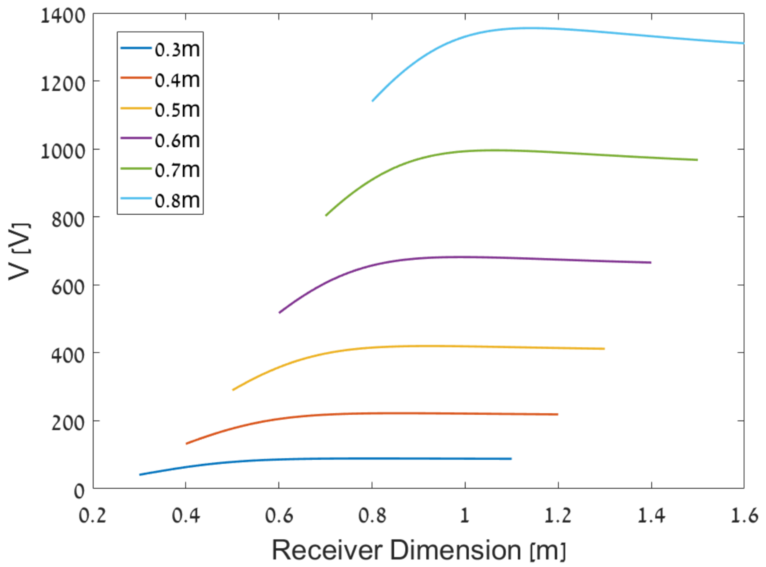

Figure 16: Length dependent receiver voltage. Different curves represent different transmitter coil dimensions from 0.3 to 0.8 m

In practice, the vehicle width has a tighter dimension restriction than its length. Hence, in the second set of simulations, coil width was fixed at the applicable value of 0.5 m and only the length of the receiver coils was varied. The results are seen in figure 16. In this case, the effect is slightly less dramatic than for the 2-directions change case; however, it is still strong. The voltage curves reach a maximum at around the same points as in the previous case and decrease in a weaker way thereafter.

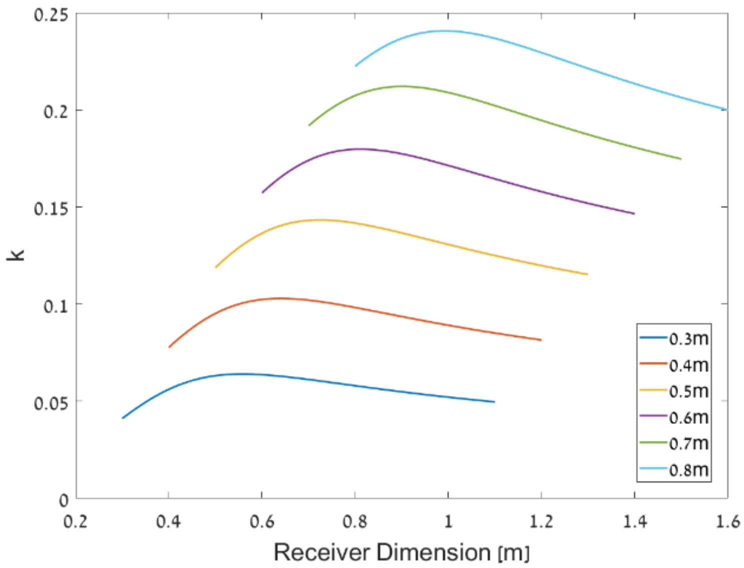

Figure 17: Coupling coefficient as a function receiver coil length. Different curves represent different transmitter coil dimension from 0.3 (lowest curve) to 0.8 m.

Figure 17 displays the coupling coefficient, k, as a function of dimension changes. The self and mutual inductances of equations 1, 2 were calculated from the voltage induced in each coil by varying the current in the appropriate coil. Clearly, k increases with the increase of the transmitter coils dimensions. For transmitting coils of 0.3 m length, k is less than 0.1 and increases up to ~0.35 for 0.8 m long coils. The optimal operation point is now clearer and corresponds to the peak in k. For any selected transmitter coil size, the coupling between the coils improves with the increase in the receiver coil length up to a maximum. Further increase in length results in decreasing k hence, reduced energy transfer efficiency. The increase in k with increasing transmitter coil size is straight forward. Since the coupling is proportional to the ratio r/h, (h being the distance between coils and r its typical dimension) [32], enlarging the transmitter coils is equivalent to reducing the distance between the transmitter and receiver coils. Therefore, it is desirable to have as large as possible transmitting coils and the limit is set by cost of the conductor, the road trenching, and the need to keep the dimension smaller than the EV width to minimize stray fields in its vicinity.

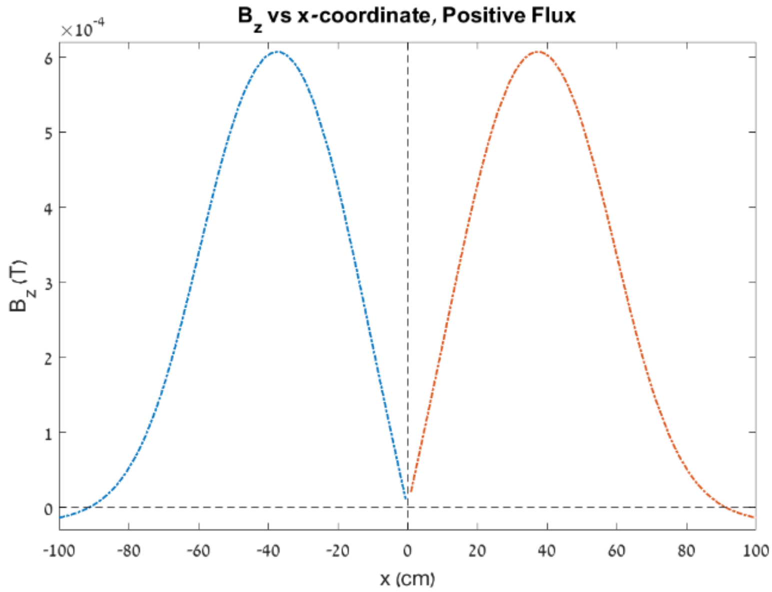

Figure 18: Position dependent B_z along the x-axis on the XY plane of the receiver. The direction of the flux displayed in this figure represents the flux that is seen by each receiver. Maxima are observed at around x = ±38 cm.

To explain the non-monotonic behavior of k for each selected transmitter size, one must examine the magnetic field distribution in the XY plane at the receiver level, and the XZ plane. Figure 18 describes the z component of the magnetic field (B_z) in the receiver coils XY plane, for the case of 0.5 m sized transmitters. B_z reaches its maximum/minimum at about x = 38 cm / -38 cm respectively. These points represent the maximum amount of flux that can be "caught" by the receiver coils. Once we venture past these points, B_z starts diminishing. Upon reaching a negative field, (at around 90 cm), the induced voltage on each receiver declines.

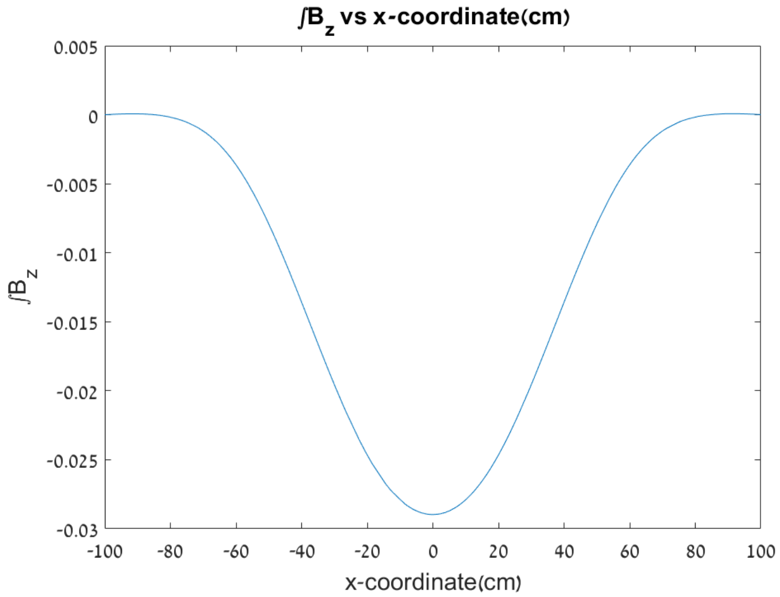

Figure 19: Integrated z component of the magnetic flux density along the x-axis.

Figure 19 represents the integral of B_z integrated over x axis (direction of motion). This figure correlates well with figures 17 and 18, as the overall flux starts plateauing rapidly at around 0.7 m. This is the point where the flux in figure 18 decreases rapidly and is about to flip and become negative, therefore obstructing further flux collection. Also, in figure 17 we see that k starts decreasing rapidly after that point, which strengthens the claim that once we go past this point, flux collection becomes negative.

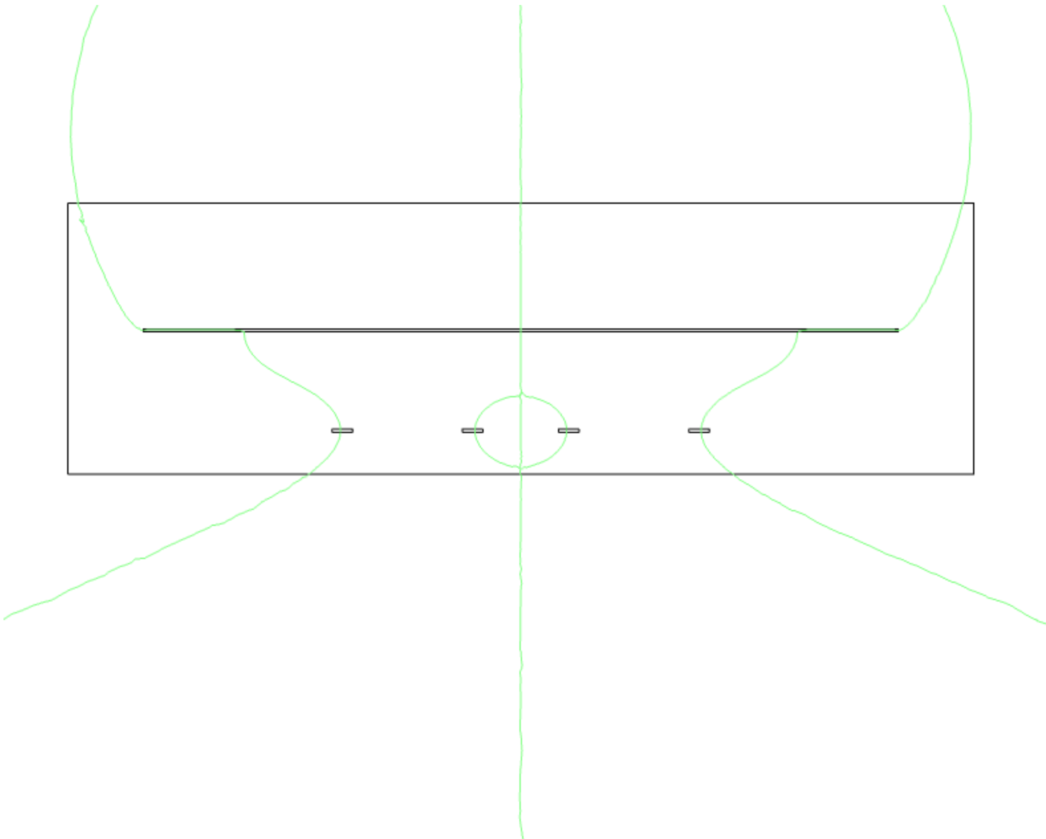

Figure 20: A side view of the system. The green line represents every point where $B_z = 0$, meaning the flux direction flips in every region.

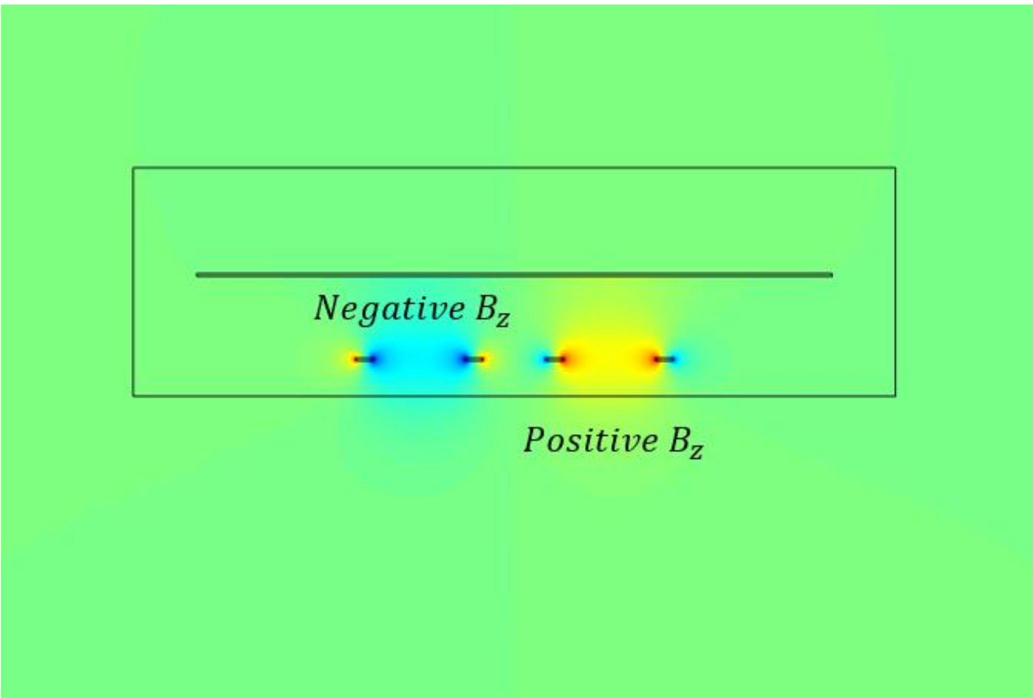

Figure 21: A side view of the system. Yellow hues represent positive z flux, while blue hues represent negative z flux.

Another way to view the flux behavior is shown in figure 20, which is focused on the XZ plane. It describes the line where the z-component of the magnetic field flips, i.e., the line where $B_z = 0$. We can also see that this line becomes horizontal inside the ferrite, since it "pulls" the flux lines into it, making the field completely horizontal. This in turn drives the $B_z = 0$ line away from the center. This also correlates well with the other results presented here. Figure 21 shows a colored version of the same phenomena. The blue hues represent the negative flux, while the yellow hues represent the positive flux. It gives a more in-depth picture of the magnitude of the flux in every given point in space.

By mapping the magnetic field that is created by our transmitter configuration, we can gather insight about the most efficient geometry for the receiver coils, which will be used in the following chapters.

5.1.3. Coil Separation

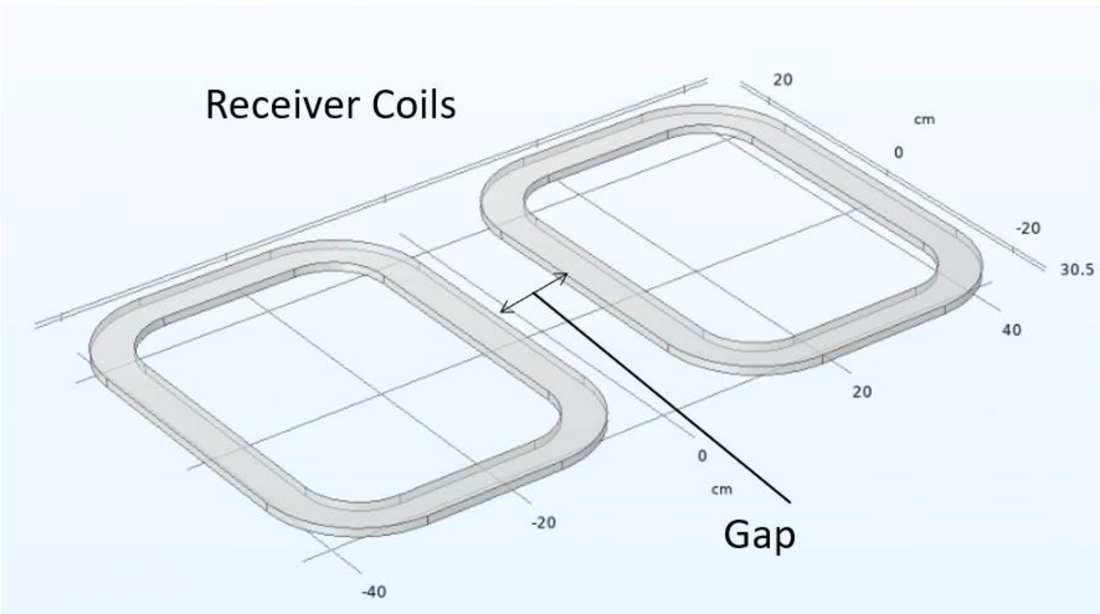

Figure 22: Added gap between the 'DD' coils.

As previously discussed, figures 18 and 19 describe the z-direction flux that is created by a set of bi-polar transmitter coils. An interesting takeaway from these plots is that there is zero flux at the center (x=0), and the contribution to the flux crossing the receiver coils array is small near this center. Looking at said figures, an idea arises to shift the 'D' frames along the x-axis so that maximal flux can be picked up. Namely, the 'DD' configuration becomes now double 'D' frames separated by a distance, as seen in figure 22.

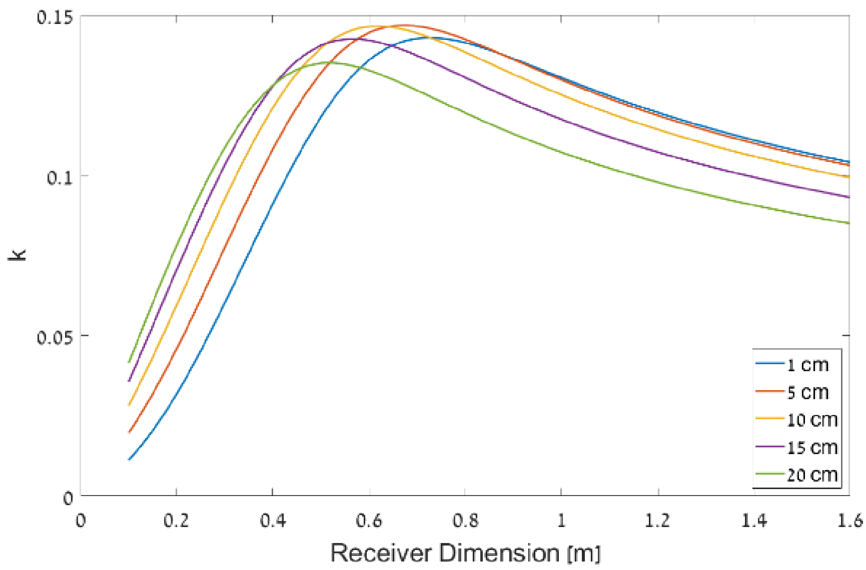

Figure 23: Comparison between different separating gaps.

It is this distance that we've next explored to further optimize the energy transfer as shown in figure 23. The figure describes the changes to k in different separation distances, ranging from 1 to 20 cm. The transmitter coils used here are the default coils of 38 cm "radius". Each line represents a different distance between the D-shaped coils. For small receiver coil dimensions, we clearly see that k increases with increasing separation. For example, for receiver coils of 0.3 m, k increases from about 0.05 for 1 cm separation to ~0.12 for 20 cm distance, nearly a 3-fold improvement! This is attributed to the expected increased flux collection as we center the "D" coil around the maxima in B_z. However, for large coils, we see a reversal of this behavior and k of smaller separation distance is higher than k of larger distances. Again, we can explain the results as the horizontal shift of the coil brings larger coils into the reversed flux region hence decreases k. We can, therefore, conclude that a separation of 10-20 cm is ideal for this case of 38 cm transmitter coils. For these separation intervals, k reaches the highest level, while also being more cost efficient than just changing the dimensions of the coils. Putting it all together, we can get an ideal 'DDQ' – type of configuration for our receiver coils that are best suited for a static case. These results are carried over to the dynamic phase of the simulations.

5.1.4. Efficiency

The maximal efficiency of an inductively coupled resonator system is given by [10]:

$$\eta_{opt} = \frac{k^2 Q_1 Q_2}{\left(1+\sqrt{1+k^2 Q_1 Q_2}\right)^2}$$

Where Q_1, Q_2 are the quality factors of the transmitter and receiver circuits, respectively. For our purposes, the calculated Q_1, Q_2, using the self-inductance and resistance of the coils in the 50 cm case, were:

$$Q_1 \approx 52.34$$

$$Q_2 \approx 467.7$$

Note that a series resistance was added to the transmitter coils, therefore reducing the Q-factor of Q_1. The resistance values used here were obtained from Electreon Ltd. to reflect realistic values of DWPT circuits used in their projects. Assuming an average 0.15 value for k, one can get a maximal efficiency of:

$$\eta_{opt} \approx 0.9183$$

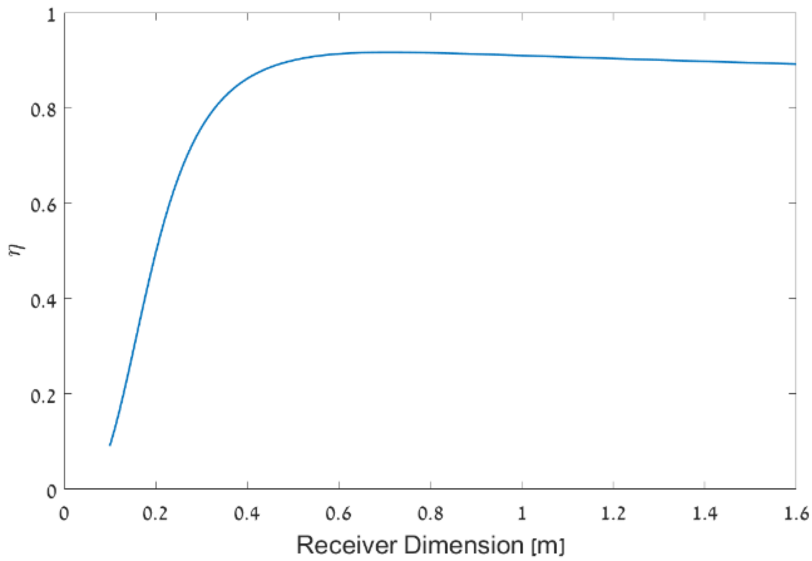

Figure 24: Energy transfer efficiency of the 10 cm separation case. It peaks at around 50-60cm, similarly to the peak in k shown in the previous figures. Unlike the previous figures however, the decline afterwards is rather small.

Figure 24 describes the changes to the efficiency as a function of the receiver coil size. The efficiency climbs steeply from about 10% for coils of 10 cm radius to about

90% for coils of about 60 cm size. A further increase in receiver size results in a slowly declining efficiency. We therefore have managed to increase the efficiency of the system from less than 80% in the completely non-optimized state (with zero coil separation), to almost 92%! Yet, again, we understand this negative slope of the efficiency as the outcome of reversed field lines penetrating the coil cross-section.

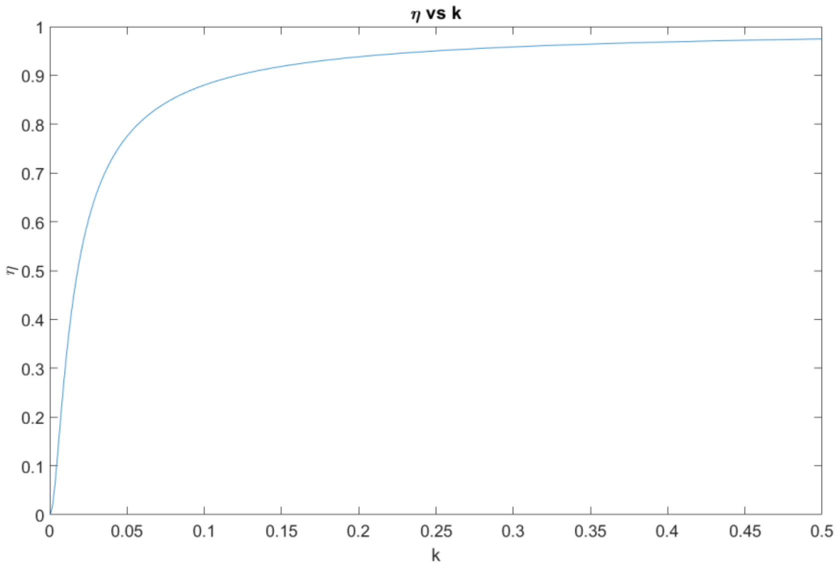

Figure 25: Efficiency changes with k. The efficiency is susceptible to changes for low k values.

Clearly, the more fundamental parameter to affect the efficiency is k. Therefore, figure 25 exhibits the k dependent efficiency. Seen here, the efficiency soars sharply with the increase in k for small k values but now the curve is monotonic. Above around 80% efficiency, the curve begins to saturate, and it becomes harder and harder to achieve efficiencies higher than the 92% efficiency we have already achieved in the stationary case. This behavior can also be seen from the equation and is evident in the figure. The efficiency is extremely susceptible to changes in the coupling coefficient k, especially when k is low. This means that during the movement of a DWPT array, even though the exact same coils are present throughout the entire time, the efficiency is going to change dynamically with respect to the location of the EV along the travel path. At high k values however, the efficiency does not change much, which is why it is so important to keep k at a relatively high value during the drive. In our work, for the range of coil dimensions explored, the efficiency is still susceptible to changes, and must be taken into account.

5.2. Non-Ionizing Radiation

This chapter is devoted to an issue of public concern: the non-ionizing radiation of EVs supported by DWPT technology. When people hear about EVs traveling along the road being charged “on the fly” by energy transmitted by coils embedded in the road, one of the first questions and reservations that pop immediately is “what about the radiation?” Naturally, we are all concerned about environmental issues that affect our lives so one critical demand from DWPT technology is that at no circumstances, passengers or stand-by pedestrians are to be exposed to radiation levels that might have any effect on their bodies, short or long-term. One aspect of this issue is resolved immediately by switching electronics. Each EV (receiver coils layout) carries a unique identifier (RFID or the sort), which signals the transmitter that the receiver is above the transmitter and exactly at what position. Only then, when the coils overlap in the x direction, energy transmission begins and stops when the EV has finished its passage. In this way, it is guaranteed that no radiation is present except for just below the EV. Two other radiation scenarios are left open: 1. The radiation from power cables, which conduct the high currents to the coils, and 2. The radiation at the passenger’s level, right above the EV chassis. In this chapter we describe simulation studies we’ve performed for such scenarios proving beyond any doubt that DWPT under the conditions explored in this work is perfectly safe, exhibiting radiation levels well-below the allowed standards.

First, we’ve simulated and measured the residual radiation over the top of the ferrite plate. As explained in the introduction, a ferrite plate covers the “DDQ” receiver coil layout for two purposes:

1. Increased coupling - being a ferromagnetic material of high permeability, this plate serves as “magnetic flux concentrator”. Less energy is required for field lines to divert its course and be attracted to the plate. Hence,

field lines that would otherwise escape the receiver coils are now attracted and tilted so that the net flux through the coils increases.

2. Radiation screen – for the same reason, residual field lines above the receiver coils are now trapped within the ferrite. The plate serves as a screen and the radiation above its physical height level is reduced.

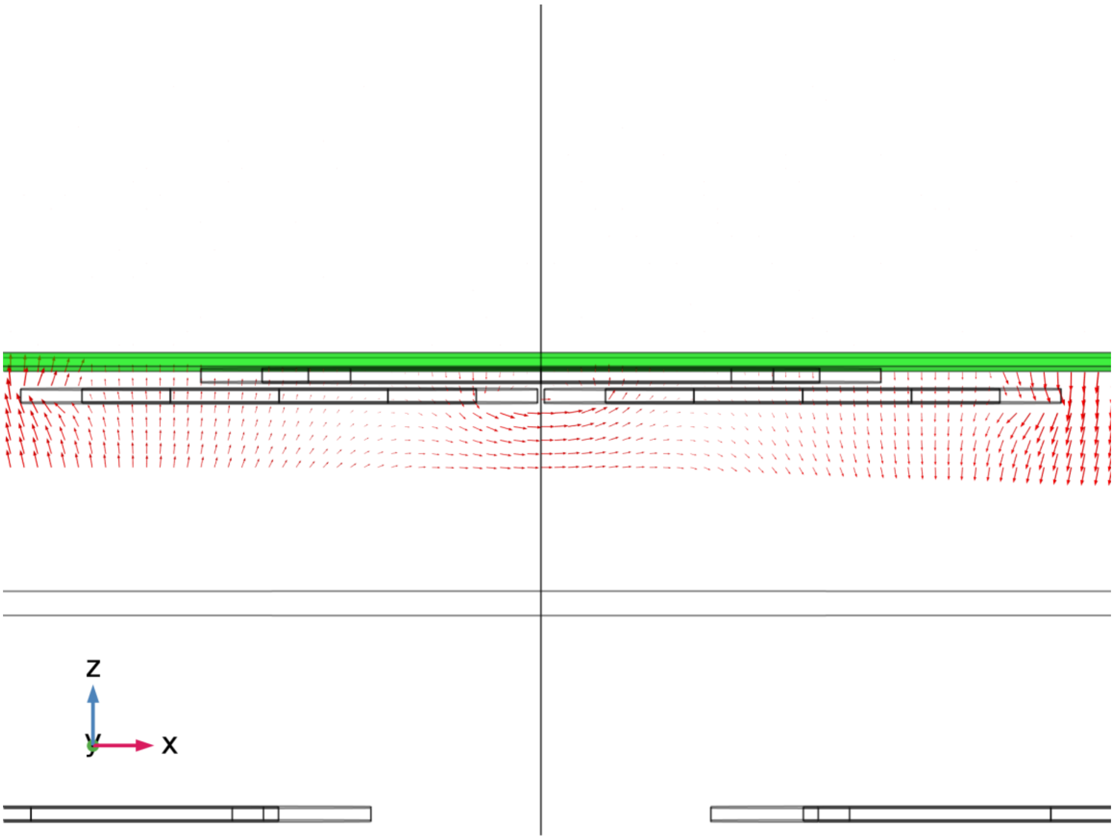

Figure 26: A side view of the system. Flux lines are drawn in proximity to the ferrite plate in a logarithmic scale, including the region above it. This means that the flux above the ferrite is orders of magnitude lower than the incoming flux.

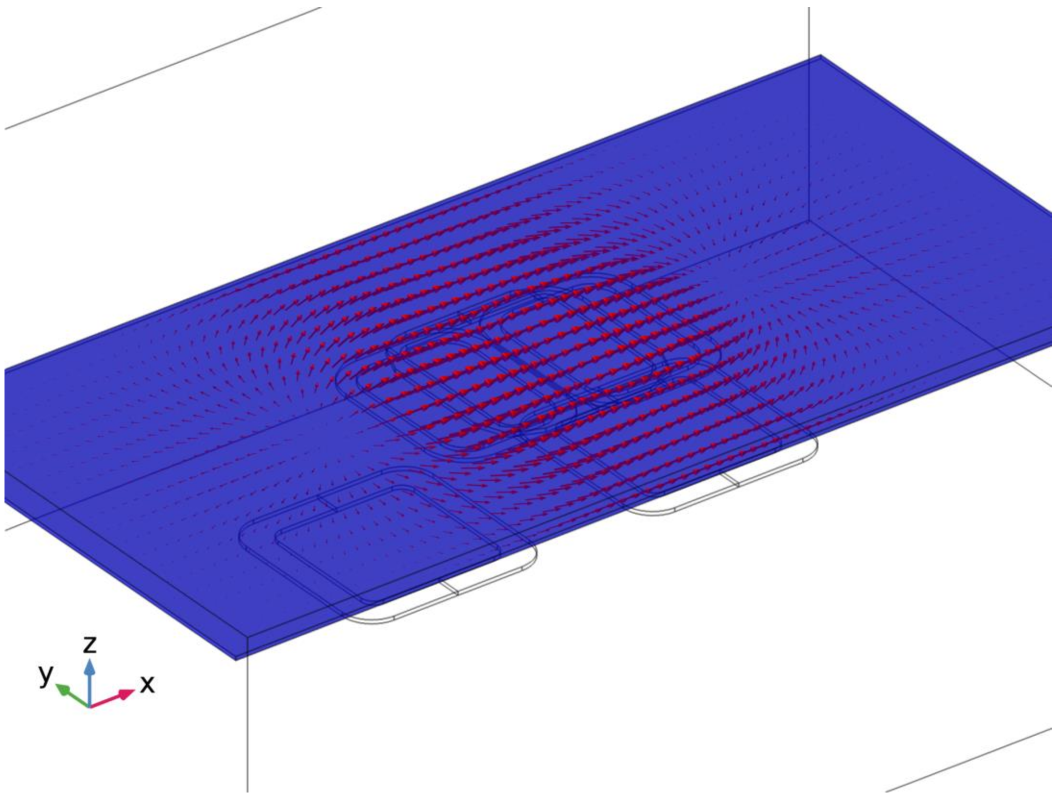

Figure 27: Flux lines inside the ferrite plate that screen the incoming radiation.

Figure 26 shows the ferrite plate in action. It shows how no flux lines penetrates through the plate to its other side (of course, given the resolution in the figure). Figure 27 describes the “pulled” magnetic flux inside the ferrite plate which blocks the magnetic flux from penetrating it. The inside flux is created due to the ferro-magnetic properties of the ferrite, which is why it acts well as a screening tool for non-ionizing radiation.

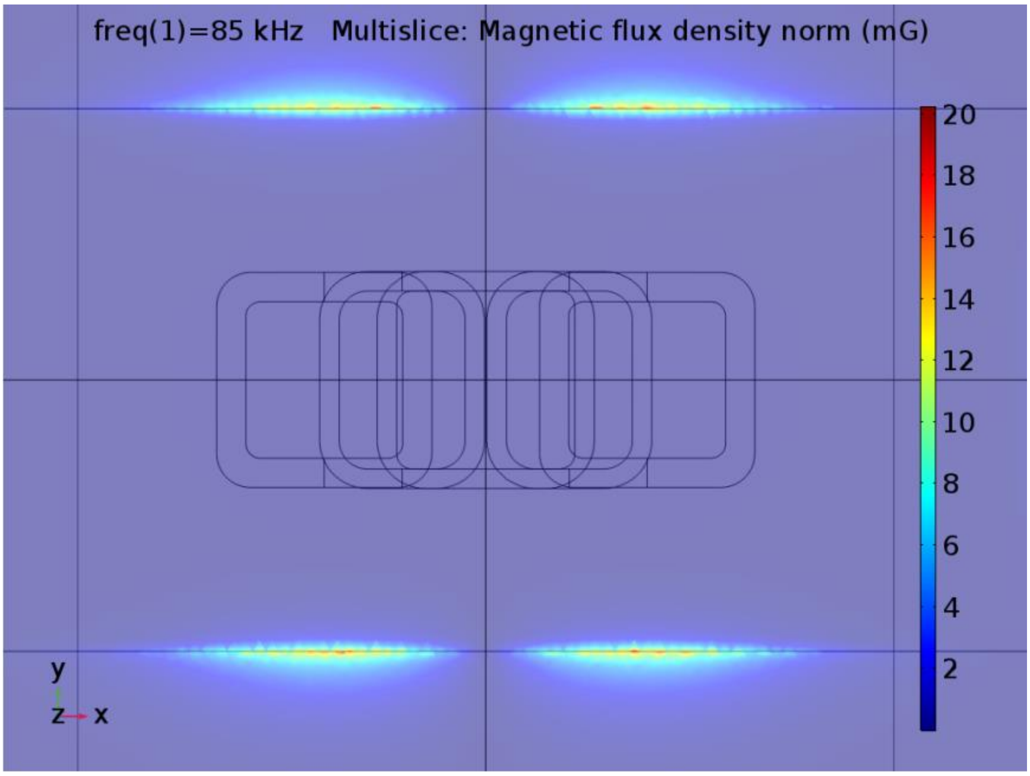

Figure 28: Radiation intensity (mG) at ferrite plate level. The maximal flux we get from the sides of the plate are well below the maximum allowed radiation levels. If needed, an aluminum plate can be placed to further reduce radiation.

The numerical results are presented in figure 28. The ferrite plate is very effective at reducing the radiation on board of the EV. The magnetic field scale depicted in this figure ranges from 0 to 20 mG and in this scale the measured radiation above the ferrite plate is effectively zero. A small, below guidelines amount of the radiation does slip through the edges of the ferrite plate, however it reaches a peak of about 20 mG, which is well below the standards for non-ionizing radiation threshold – 270 mG [27] at 85kHz Also, if needed, an aluminum cover can easily be placed to further reduce the radiation regardless, which can cancel the residual radiation. The addition of an aluminum plate will create eddy-currents when exposed to AC magnetic flux, which can be extremely efficient at screening the flux all-together. Another way to reduce radiation, without the use of external aluminum plates, is to change the geometry of the ferrite itself and increase the screening. This can be done in several different ways, for instance, making the edges of the ferrite thicker or inclined, which will contribute to the screening. It is worth mentioning that we save the Aluminum plate addition only if truly required since its screening by eddy-current generation results in losses that reduce the efficiency.

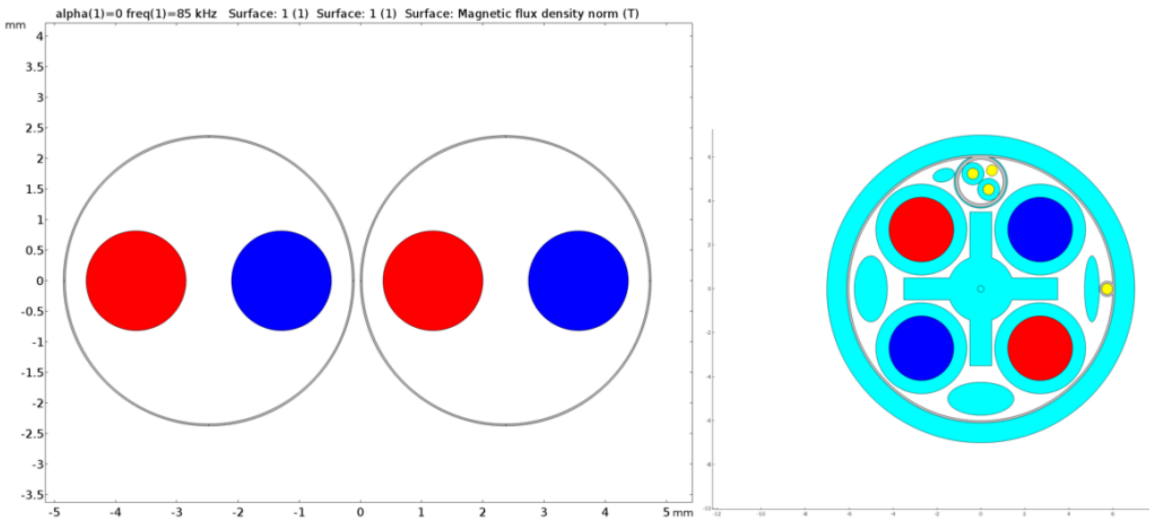

Figure 29: Simulated model of the cross-section of the cables. Left: Double twisted cable. Right: 4C cable. The red and blue colors represent positive and negative terminals respectively.

Second, we've simulated the underground cables that carry the current to the transmitter coils. We've simulated two types of cables, typically used for high-power high-frequency applications: the double twisted, and 4C cables shown in figure 29. Cables are made from Litz wires namely, multi filaments twisted for reduced eddy-currents and homogenous current flow within its cross-section. To simplify the simulations, we've simulated a single filament cable since at the distance of interest, one may neglect the internal structure of the cable. The cables are embedded in depth of about 50-60 cm below the ground, therefore it is important to make sure that they do not emit harmful levels of non-ionizing radiation at the ground level and above.

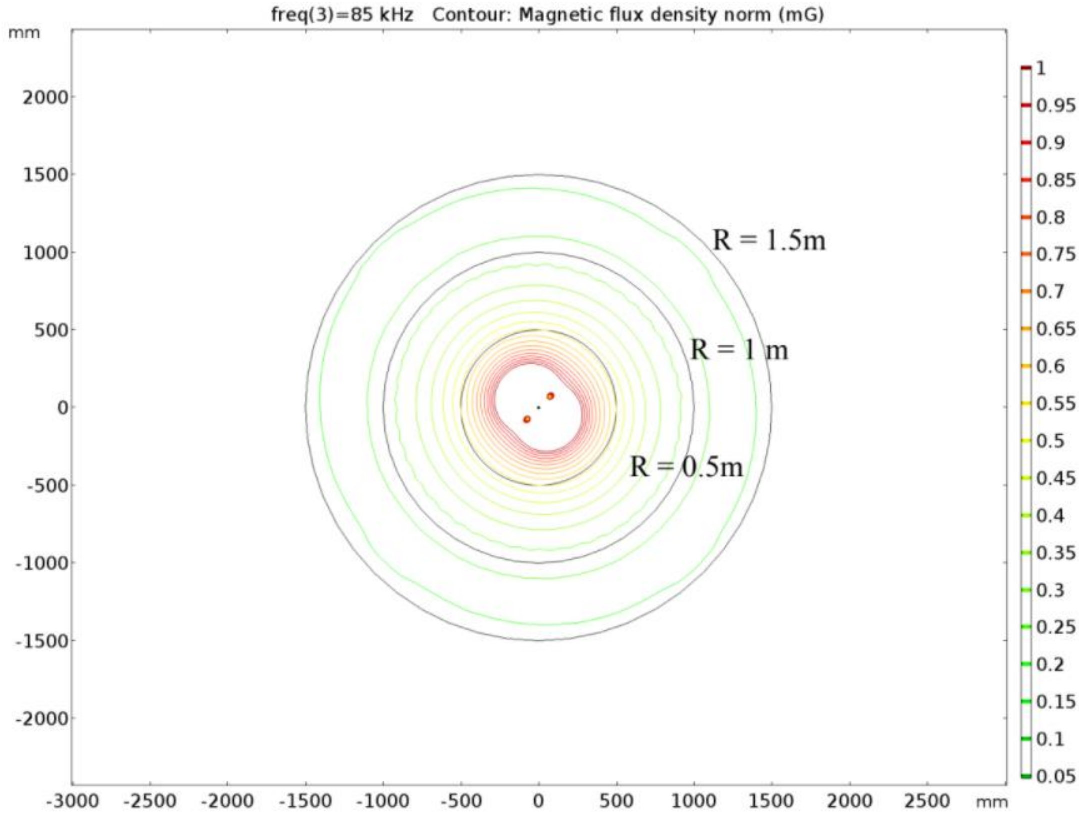

Figure 30 : Flux lines at 0.5m, 1m and 1.5m away from the cable. The lack of symmetry around the cable is a direct result of the opposite terminals of the cable, as seen in the previous figure.

Figure 30 describes the radiation around the 4C cable. The radiation symmetry close to the cable itself is broken, as the current moves in and out of the terminals in a quadrupole type of configuration. At 50 cm, the radiation is symmetrical and is well below the threshold, at about 0.4 mG.

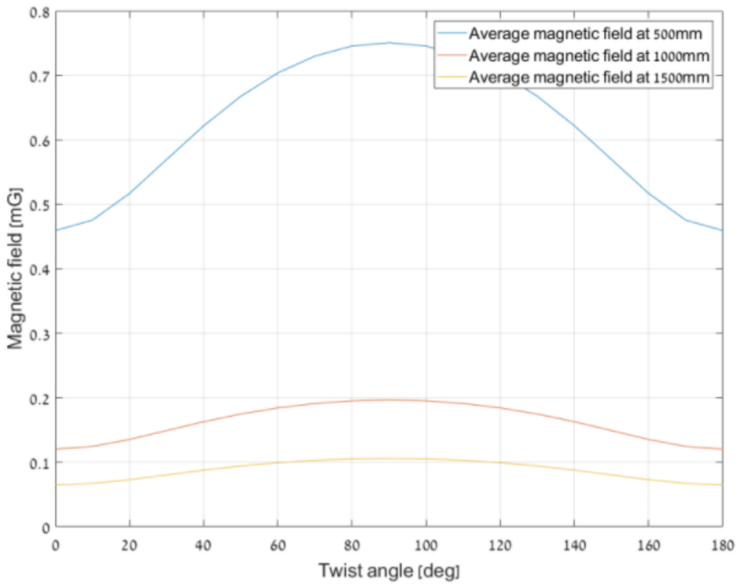

Figure 31 : Twist angle distribution of the flux in the double twisted cable. The x-axis represents the twist angle of the cable. The y-axis represents the residual average magnetic flux at different heights above the cable. At 0.5m the radiation is well below the allowed radiation levels.

Figure 31 describes the radiation around the double twisted cable at various twist angles. The radiation is the strongest at 90 degrees of twist, since the configuration switches from a state of quadrupole to a state of a dipole, increasing emitted flux. The radiation at 50 cm is also well below the threshold, even at 90 degrees, where the radiation is maximal at about 0.7 mG.

In summary, the non-ionizing radiation emitted by the transmitting circuit fall well below the allowed standards both for the coils and for the current carrying cables. If, in the future, the standards are toughened, we see easy ways to further reduce the radiation levels. We therefore conclude that DWPT, in the layout explored in this work, is safe for use.

5.3. Dynamic Results

In the previous chapters we've described an optimization study for increasing the coupling coefficient and the energy transfer efficiency. However, the EV and the receiver coils array travel along its rout and the relative distance between the transmitter and receiver coils change all the time. Variations in the relative positions of both set of coils might occur in all 3-dimentions. Not only that the EV progresses along its travel line thus changing the coil position along x-axis, but transverse deviations from the charging path are inevitable. Height fluctuations are also likely to be present in any real-world drive due to imperfections in the road and variations in passenger's weight.

Therefore, we hereafter present a study of the coil layout under dynamic conditions and explore the coupling coefficient, resonance frequency and energy transfer efficiency when the relative position between coils is changed in all axes.

5.3.1. Initial Configuration

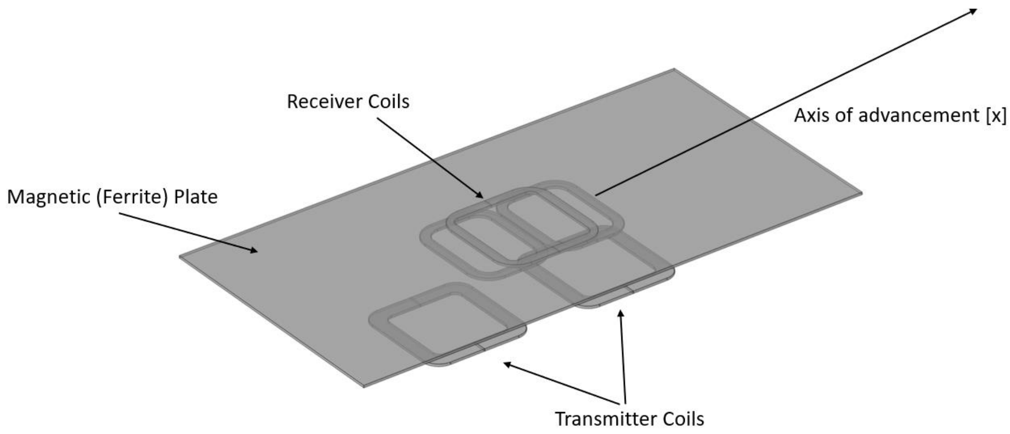

Figure 32 : Baseline configuration for the dynamic simulations. The axis of advancement is dubbed 'x' for the rest of this work.

A similar type of configuration that was used in the static simulations can be seen in figure 32 and is used as a baseline for our dynamic simulations. In these simulations, we've simulated an EV moving along a travel path, as well as possible misalignments in the other axis.

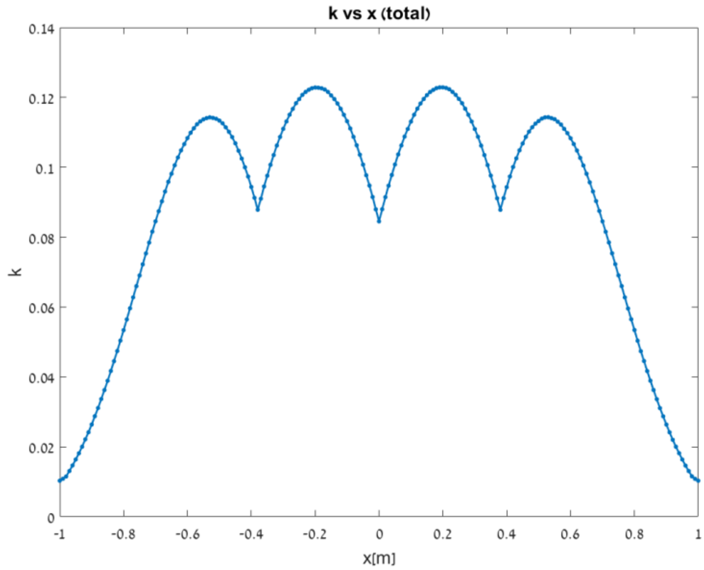

Figure 33: Changes to k at different x-axis misalignments. Consistently good k values are obtained throughout the entire movement.

The changes that occur to k along the travel path of an EV can be seen in figure 33. The 'DDQ' configuration proves to have a good flux collection coverage, however, the fluctuations in k are very significant in these levels and can greatly affect the transfer efficiency as seen in figure 25. The takeaway message here is that we cannot assume that a single k value is carried throughout the entire segment of charging, as it is simply not the case. ‘k’ changes dynamically, and we must take that into account.

5.3.2. Improved configurations

The most obvious change to be made to the configuration, based on the previously mentioned static cases, is to increase the spacing between the 'DD' coils as was demonstrated in figure 22.

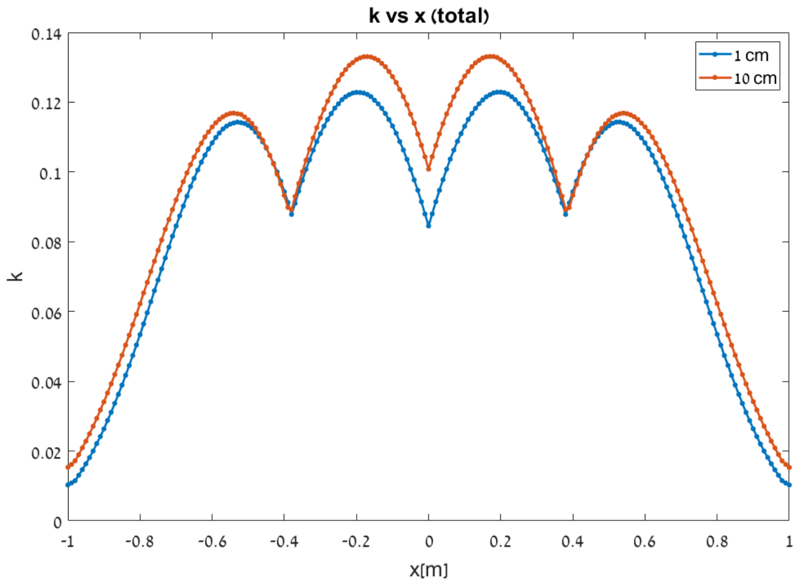

Figure 34: Changes to k at different x-axis misalignments for two spacing options – the default 1 cm case, and the 10 cm case, the latter being superior in every single way.

Figure 34 demonstrates how the 10 cm spacing case (red curve in the figure) is superior in every way to the minimal 1 cm spacing case (blue curve), as k remains relatively higher along the entire path.

This again sits well with figures 18 and 19 mentioned in the static section – more flux can be collected if we place the 'DD' coils away from the center. This is since the z-component of the magnetic field is far weaker at the center than it is about 40 cm away from the center. Spacing the receiver coils away from each other is a logical conclusion that can be drawn from that fact – and it was indeed proven to be effective, increasing flux collection throughout the entire drive.

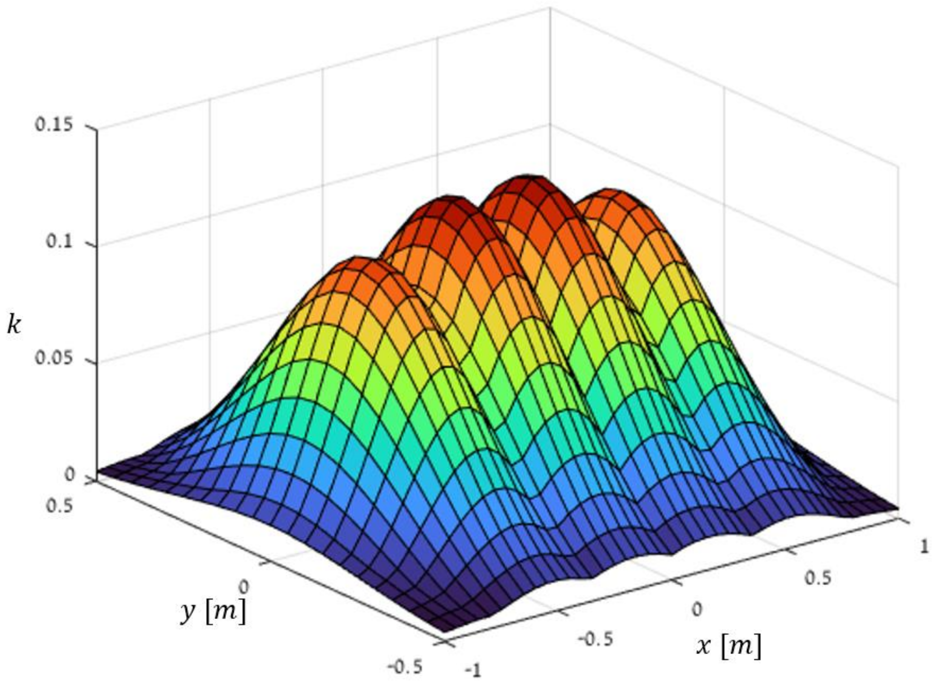

Figure 35: x-y mapping of k as a function of the misalignment in the x and y axes.

For the 10 cm spacing case we've also mapped an x-y plane as seen in figure 35, where each point on the grid represents k in different locations on this plane. We can see that misalignments in y also play a big role in affecting the amount of flux collected during the drive. For example – a 10 cm misalignment in the y-axis can decrease k by up to 25%. Since these kinds of misalignments are bound to happen constantly during drives, it must be taken into consideration when designing DWPT systems, which can result in more transmitter coils per length unit to be needed or by increasing the on-board battery. A z-axis misalignment can also greatly affect k and has been done in previous works [32].

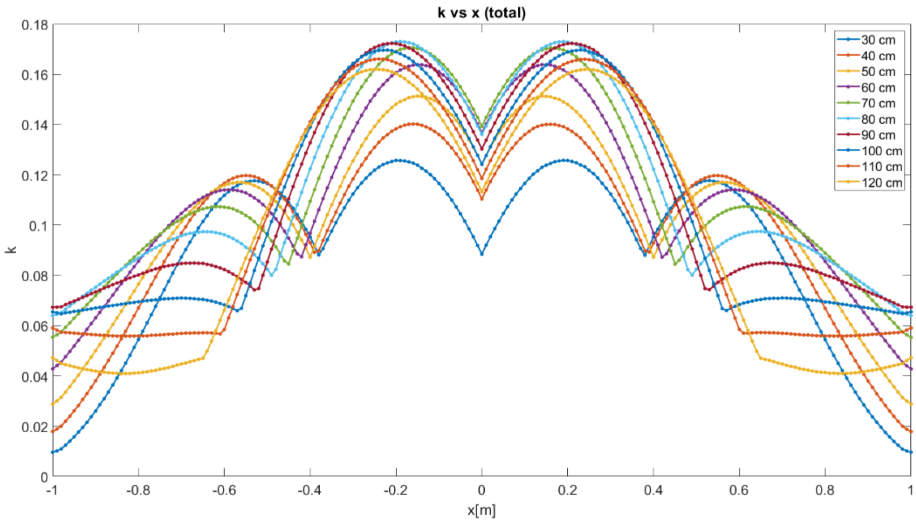

Figure 36: Changes to k dynamics with different sized coils.

Next, we made the same stretching simulations presented in the previous section but now on a dynamic system. The results are presented in figure 36. These dynamic simulations have produced several interesting insights about the system. First, we see that the maximal achievable coupling coefficient is not only higher at 25 cm along the travel path, but also corresponds to a different receiver coil size than previously predicted in the static case. This sits well with the results previously shown in figure 18, as the peaks in k occur where the receivers fully encapsulate the magnetic flux generated by the transmitters. Furthermore, we can see that the larger the coil, the more flux is collected in the center of the x-axis and is less collected at the edges of the transmitter array. The main takeaway from this figure is that for smaller coils, the collected flux is smaller but spread-out more evenly throughout space. For flux maximization, one must use the larger coils, at the cost of low efficiency at the edges of the array.

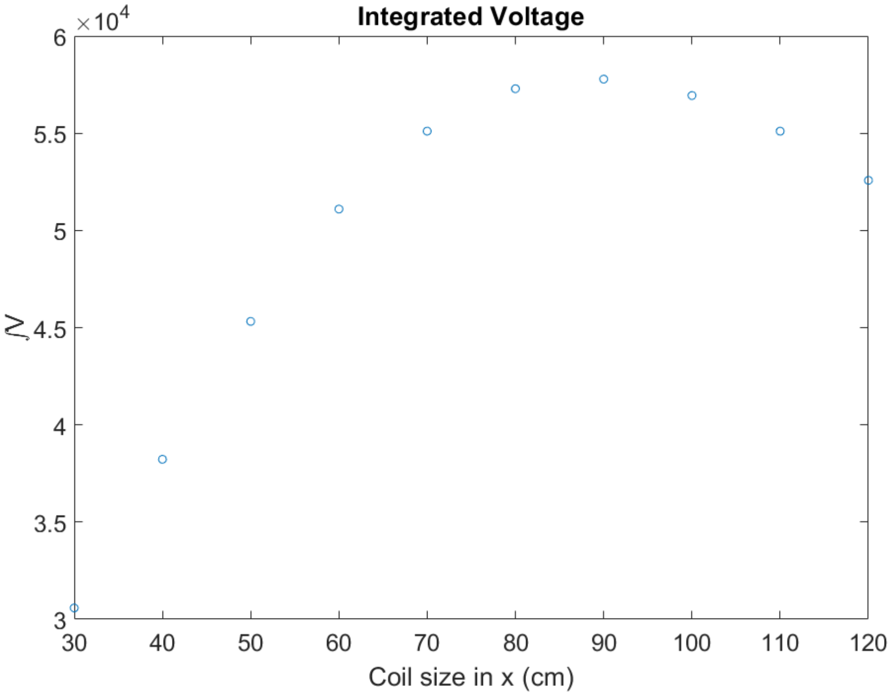

Figure 37 : Total integrated voltage for each size case. The maximum voltage was accumulated in the 90 cm case.

We have also integrated the total induced voltage in every presented case to get an idea of the total collected flux of each curve, the results of which are presented in figure 37. We can see that the best configuration – the one that will collect the most flux during the drive along the track – is the 90cm case. These results are very important for our understanding of DWPT, as previous works did not account drastic changes to geometry dimensions in the context of dynamic charging. The results that we have obtained give us a clear, optimal working point for the dimensions of 'DDQ' configurations. Not only can we maximize k, but we can also extrapolate other important parameters out of these changes to k, such as efficiency (as seen in previous chapters) and even the resonance frequency changes (as is presented in the next chapter).

5.4. Resonant Splitting

In the introductory chapters, we've seen how the efficiency of DWPT system is derived from the coupled electromagnetic equations assuming that the two sets of coils operate under an identical self-resonance frequency. At present, DWPT technology operates under the assumption that indeed, the resonance frequency is constant throughout the travel and is identical for both circuits. Selected capacitors are added to both transmitter and receiver circuits precisely to match both circuits self-resonance-frequency. However, the results presented in the previous chapter for the dynamic properties of DWPT suggest that this assumption may be unrealistic. As the vehicle passes above the transmitting coils, the mutual inductance between the coils becomes position dependent. As a result, k becomes position dependent as well hence, we are facing a case study of loosely coupled oscillators where the coupling itself is dynamic. It is therefore the goal of this chapter to explore the energy transfer process under the realistic conditions where k fluctuates along the EV passage, and one cannot assume anymore a constant and fixed resonance frequency. Since the coupled equations of chapter 2.3 are not solvable analytically, we've implemented our simulation tool to solve the case numerically.

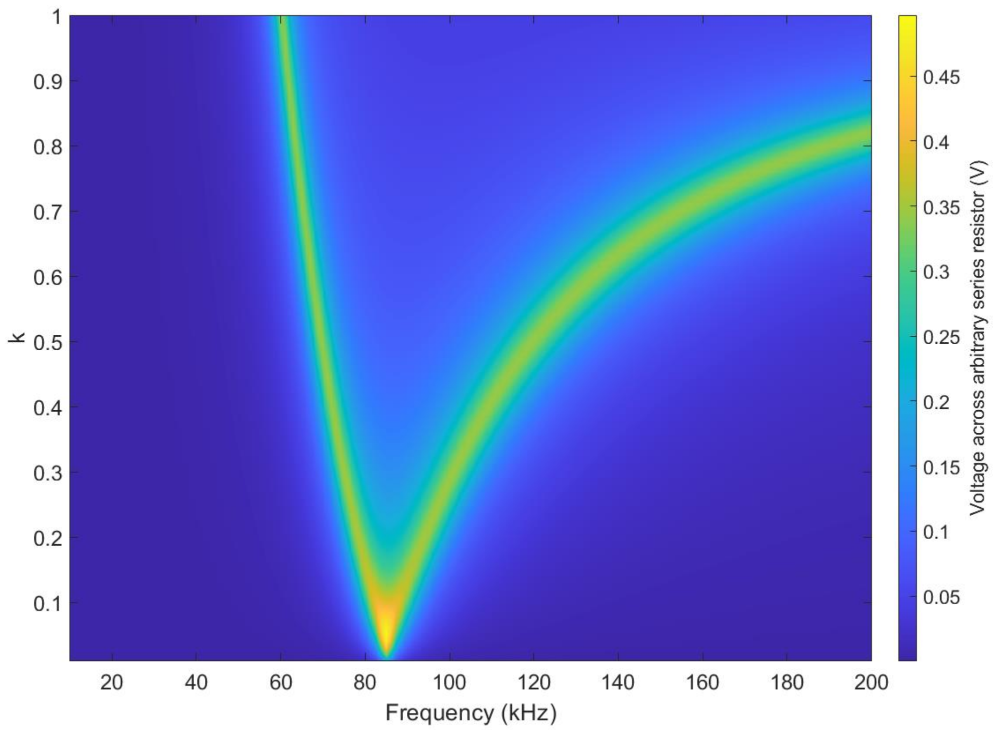

Figure 38: Resonance split occurs if the coupling becomes strong enough. The x-axis represents the resonance frequency of the system. The y-axis represents the coupling coefficient. The color-bar represents the effective voltage induced in the receiver coils. Instead of a single resonance frequency, two applicable resonance frequencies emerge. This must be considered when designing the electronics and circuitry of DWPT systems.

During our simulations, we've shown that the resonant frequency of the coupled system splits in two. We've tested the extent of this phenomena in a separate simulation. The split is visible in figure 38, where we see a clear divergence from the 85kHz initial tuned resonance frequency into two separate frequencies at around $k \approx 0.11$. This is rather unintuitive, as we always strive for high k values, which, as seen in previous sections of this work, is directly responsible for both the general power transfer of the system, as well as the power transfer efficiency, can 'kick' us out of resonance unintentionally. As seen in the previous sections of this work, the coupling coefficient far exceeds this value on a regular basis. The fact that the resonance of the receiver changes when driving is an incredibly important matter that must be compensated for, as the whole concept of DWPT rests upon the idea of magnetic resonance power transfer. A system that is off resonance will not benefit from the huge amplification it receives from the quality factors of the receiver and transmitter systems. Therefore, active resonance tuning must be implemented into the system via dynamic circuitry methods, such as active capacitance changing feedback loop.

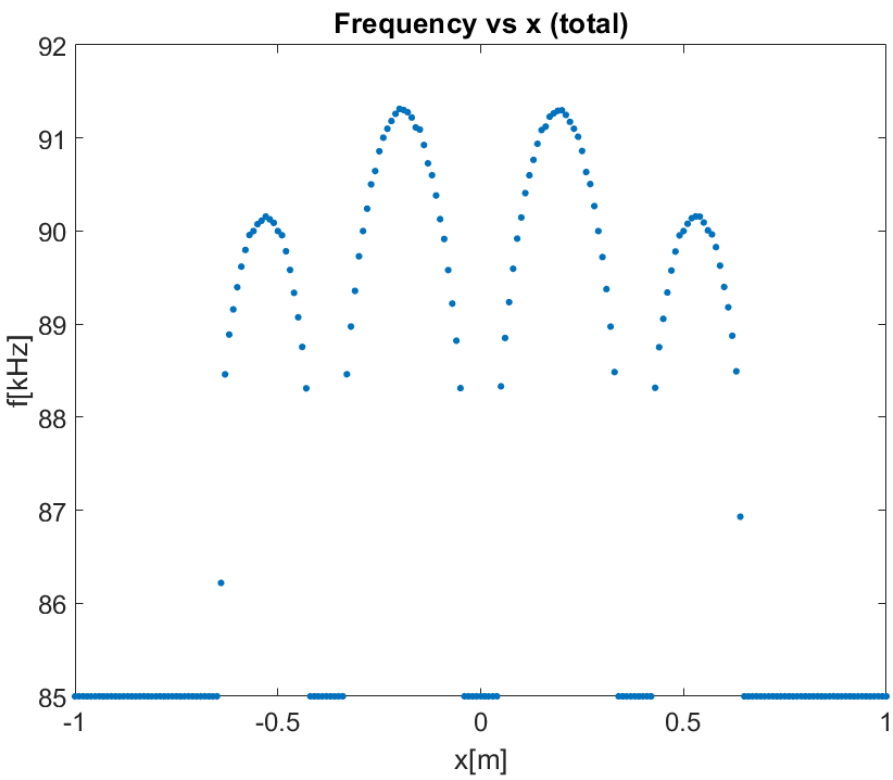

Figure 39 : Changes to the resonance frequency with misalignments in x for the initial configuration. Drastic changes to the resonance frequency are observed as k peaks.

For the scope of this work, we have decided to map these changes in resonance on the driving axis of the EV. These results are presented in figure 39. This, in turn, not only severely reduces the energy transfer, but also changes the efficiency of the system if no action is taken.

6. Conclusions

This work focused on achieving improved energy transfer efficiency in DWPT technology. To do so, the effects of different configurations of coils in DWPT systems, in both the static and dynamic cases, have been studied. Specifically, we have explored the coupling coefficient between the road embedded transmitter coils and the chassis bound receiver coils, and the levels of non-ionizing radiation.

In the static case, we have found that an optimal size for receiver coils exists for every selected size of the transmitter coils. The coupling coefficient increases with increasing receiver size, peaks at this optimal size, and decreases thereafter. We have also found that a similar optimization can be done by creating a gap between the 'DD' receiver coils, resulting in better flux collection. These findings were interpreted by analyzing the spatial magnetic field distribution, which have shown that the net magnetic flux which crosses the receiver coils start to decrease above the optimal dimension and gap due to magnetic field direction reversal. The coupling coefficient in turn can be directly translated to power transfer efficiency.

Non-Ionizing radiation was analyzed in all potential hazardous parts of a DWPT systems, including the coils and high-current carrying cables used in such systems. All non-ionizing radiation was determined to be well below the threshold, mainly thanks to the ferromagnetic ferrite plate place below the chassis of the EV, which is used also for radiation screening. Regardless, if needed, further screening methods can easily be employed to further reduce non-ionizing radiation if needs be, as discussed in chapter 5.2.

In the dynamic case, we have shown how the proposed optimizations made in the static case work in a drive scenario. We have shown that, during motion, the optimized static configuration is not the optimal configuration for a dynamic situation. We have also shown how different misalignments on the axis perpendicular to the drive affects the coupling coefficient at all times.

Finally, we have shown that during the drive, the dynamic nature of the coupling coefficient greatly affects not only the efficiency of the power transfer, but also the resonance frequency of the receiver circuit, resulting in significant losses if no action is taken to dynamically adjust the resonance of the receiver circuit.

We believe that the results presented in this work can be used to further improve DWPT systems currently in development and shed some light on lesser addressed problems of DWPT, such as resonance splitting.

7. Bibliography

[1] K. Young, C. Wang, K. Strunz, and others, *Electric Vehicle Battery Technologies*, in *Electric Vehicle Integration into Modern Power Networks* (Springer, 2013), pp. 15–56.

[2] M. Redelbach, M. Klötzke, and H. E. Friedrich, *Impact of Lightweight Design on Energy Consumption and Cost Effectiveness of Alternative Powertrain Concepts*, (2012).

[3] Chevrolet, *Chevrolet EV Recall*, (2021).

[4] Forbes, *The Lack of EV Charging Stations Could Limit EV Growth*, (2021).

[5] K. Qian, C. Zhou, M. Allan, and Y. Yuan, *Modeling of Load Demand Due to EV Battery Charging in Distribution Systems*, IEEE Trans. Power Syst. **26**, 802 (2010).

[6] J. C. Gómez and M. M. Morcos, *Impact of EV Battery Chargers on the Power Quality of Distribution Systems*, IEEE Trans. Power Deliv. **18**, 975 (2003).

[7] O. Shimizu, S. Nagai, T. Fujita, and H. Fujimoto, *Potential for CO2 Reduction by Dynamic Wireless Power Transfer for Passenger Vehicles in Japan*, Energies **13**, 3342 (2020).

[8] G. A. Covic and J. T. Boys, *Inductive Power Transfer*, Proc. IEEE **101**, 1276 (2013).

[9] Wikipedia, *Wireless Power Transfer*, Wikipedia (2021).

[10] Z. Zhang, H. Pang, A. Georgiadis, and C. Cecati, *Wireless Power Transfer—An Overview*, IEEE Trans. Ind. Electron. **66**, 1044 (2018).

[11] A. Kurs, A. Karalis, R. Moffatt, J. D. Joannopoulos, P. Fisher, and M. Soljačić, *Wireless Power Transfer via Strongly Coupled Magnetic Resonances*, Science (80-.). **317**, 83 (2007).

[12] Y. D. Ko and Y. J. Jang, *The Optimal System Design of the Online Electric Vehicle Utilizing Wireless Power Transmission Technology*, IEEE Trans. Intell. Transp. Syst. **14**, 1255 (2013).

[13] S. Das, K. Pal, P. Goswami, and M. A. K. Kerawalla, *Wireless Power Transfer in Electric Vehicles*, Int. J. Appl. Environ. Sci. **13**, 643 (2018).

[14] S. Lee, J. Huh, C. Park, N.-S. Choi, G.-H. Cho, and C.-T. Rim, *On-Line Electric Vehicle Using Inductive Power Transfer System*, in *2010 IEEE Energy Conversion Congress and Exposition* (2010), pp. 1598–1601.

[15] S. Y. Choi, B. W. Gu, S. Y. Jeong, and C. T. Rim, *Advances in Wireless Power Transfer Systems for Roadway-Powered Electric Vehicles*, IEEE J. Emerg. Sel. Top. Power Electron. **3**, 18 (2014).

[16] C. C. Mi, G. Buja, S. Y. Choi, and C. T. Rim, *Modern Advances in Wireless Power Transfer Systems for Roadway Powered Electric Vehicles*, IEEE Trans. Ind. Electron. **63**, 6533 (2016).

[17] M. Kavitha, P. B. Bobba, and D. Prasad, *Effect of Coil Geometry and Shielding on Wireless Power Transfer System*, in *2016 IEEE 7th Power India International Conference (PIICON)* (2016), pp. 1–6.

[18] W. Zhang, J. C. White, A. M. Abraham, and C. C. Mi, *Loosely Coupled Transformer Structure and Interoperability Study for EV Wireless Charging Systems*, IEEE Trans. Power Electron. **30**, 6356 (2015).

[19] T. C. Beh, T. Imura, M. Kato, and Y. Hori, *Basic Study of Improving Efficiency of Wireless Power Transfer via Magnetic Resonance Coupling Based on Impedance Matching*, in *2010 IEEE International Symposium on Industrial Electronics* (2010), pp. 2011–2016.

[20] B. H. Waters, B. J. Mahoney, G. Lee, and J. R. Smith, *Optimal Coil Size Ratios for Wireless Power Transfer Applications*, in *2014 IEEE International Symposium on Circuits and Systems (ISCAS)* (2014), pp. 2045–2048.

[21] N. P. Suh, D.-H. Cho, and C. T. Rim, *Design of On-Line Electric Vehicle (OLEV)*, in *Global Product Development* (Springer, 2011), pp. 3–8.

[22] ELECTREON, *Electreon Website*, (2021).

[23] ELECTREON, *Smart Road Gotland*, (2020).

[24] S. Jeong, Y. J. Jang, and D. Kum, *Economic Analysis of the Dynamic Charging Electric Vehicle*, IEEE Trans. Power Electron. **30**, 1 (2015).

[25] J. Huh, S. W. Lee, W. Y. Lee, G. H. Cho, and C. T. Rim, *Narrow-Width Inductive Power Transfer System for Online Electrical Vehicles*, IEEE Trans. Power Electron. **26**, 3666 (2011).

[26] S. Y. Choi, S. Y. Jeong, B. W. Gu, G. C. Lim, and C. T. Rim, *Ultraslim S-Type Power Supply Rails for Roadway-Powered Electric Vehicles*, IEEE Trans. Power Electron. **30**,

6456 (2015).

[27] J. Lin, R. Saunders, K. Schulmeister, P. Söderberg, A. Swerdlow, M. Taki, B. Veyret, G. Ziegelberger, M. H. Repacholi, R. Matthes, and others, *ICNIRP Guidelines for Limiting Exposure to Time-Varying Electric and Magnetic Fields (1 Hz to 100 KHz).*, Health Phys. **99**, 818 (2010).

[28] G. A. Covic, J. T. Boys, M. L. G. Kissin, and H. G. Lu, *A Three-Phase Inductive Power Transfer System for Roadway-Powered Vehicles*, IEEE Trans. Ind. Electron. **54**, 3370 (2007).

[29] M. Budhia, G. Covic, and J. Boys, *Magnetic Design of a Three-Phase Inductive Power Transfer System for Roadway Powered Electric Vehicles*, in *2010 IEEE Vehicle Power and Propulsion Conference* (2010), pp. 1–6.

[30] C. Multiphysics, *Introduction to Comsol Multiphysics®*, COMSOL Multiphysics, Burlington, MA, Accessed Feb **9**, 2018 (1998).

[31] O. C. Zienkiewicz, R. L. Taylor, and J. Z. Zhu, *The Finite Element Method: Its Basis and Fundamentals* (Elsevier, 2005).

[32] Y. Gao, A. Ginart, K. B. Farley, and Z. T. H. Tse, *Misalignment Effect on Efficiency of Wireless Power Transfer for Electric Vehicles*, in *2016 IEEE Applied Power Electronics Conference and Exposition (APEC)* (2016), pp. 3526–3528.

תקציר

טכנולוגיית הטעינה האלחוטית הדינמית פותחת את האפשרות לטעינת הסוללה הפנימית ברכב חשמלי בזמן נסיעה על מסלול בו מוטמנים סלילי שידור. ברכב, מתחת למרכב, נמצאים סלילי קליטה. הצימוד, המבוסס על השראות אלקטרומגנטית של מערכות הקליטה והשידור, נעשה בצורה דינמית, המאפשרת טעינת רכבים חשמליים תוך כדי הנסיעה וללא צורך לעצור לצורך הטעינה. העובדה כי האנרגיה משודרת אל הרכב בזמן נסיעתו מאפשרת שימוש בסוללות פנימיות קטנות משמעותית בגודלן, קיבולתן ומשקלן ביחס לאלו הקיימות ברכבים חשמליים היום. הקטנת הסוללות מגדילה באופן דרמטי את החיסכון האנרגטי של רכבים חשמליים עקב הפחתת משקל הרכב. כמו כן, שינוי זה טומן בחובו יתרונות סביבתיים בזכות הקטנת פליטות פחמן דו חמצני (פד"ח) בזמן יצור הסוללה והפחתת פסולת רעילה ומסוכנת בסיום חייה.

עבודת מחקר זו מתמקדת בתהליך העברת האנרגיה בין סלילי השידור והקליטה מתוך מטרה לשפר את היעילות ולהביא את הטכנולוגיה לרמה המאפשרת מימוש נרחב שלה בעולם התחבורה החכמה. לצורך זה אנו חוקרים את הצימוד האלקטרומגנטי בין סלילי השידור לקליטה תוך בחינה של תצורות שונות של סלילים אלו. ביצענו שינויים במימדי הסלילים המרכיבים את המערכת ובריווח בין הסלילים, וההשפעה של השינויים הללו על טיב העברת האנרגיה של המערכת. המחקר התייחס למקרים בהם התצורה הנבחנת נייחת כלומר, הפרמטרים הגיאומטריים המגדירים את המרחק בין הסלילים קבועים וכן בתצורה דינמית דהיינו, כאשר המערכת בתנועה ו/או כאשר קיימת סטייה בין המרחק האופטימלי לזה המתקיים במציאות.

המחקר בוצע בעזרת שימוש בסימולציות אלקטרומגנטיות בשיטת האלמנטים הסופיים. הצלחנו לשפר את מערכת הטעינה האלחוטית הדינמית ואת טיב העברת האנרגיה בין מערכת השידור לרכב החשמלי. הראינו כי מתוך הבנת ההתפלגות המרחבית של השדה המגנטי ניתן לבנות מערכי שידור וקליטה בהם מקסימום שטף מגנטי נאסף. מקסימום זה מתקבל בממדי סלילי קליטה מסוימים המתאימים לנקודה בה השדה שיוצר סליל השידור מתהפך. בתנאים המיטביים אותם הגדרנו, הראינו כי במערכת נייחת ניתן להגיע ליעילות העברת אנרגיה בין הכביש לרכב הגבוהה מ-92%! זאת לעומת יעילות של פחות מ-80% לפני האופטימיזציה. כמו-כן, הראינו כי במערכת העברת אנרגיה דינמית, קבוע הצימוד משתנה בזמן התנועה וכתוצאה מכך תדר הרזוננס העצמי מתפצל. פיצול זה מתואר כאן לראשונה במערכות טעינה אלחוטית דינמית והוא צפוי להשפיע משמעותית על תכנון המערכות העתידיות.

בנוסף, חקרנו את רמת הקרינה הבלתי מייננת במערכת, והשתמשנו בסימולציות כדי לבחון

מערך אלקטרומגנטי הכולל לוח פרומגנטי המפחית את רמות הקרינה במרחב בו עלולים להימצא אנשים. רמות הקרינה שמדדנו במערך שהצענו נמוכות משמעותית מהתקן הנהוג. המחקר המתואר מציע דרכים חדשות לאופטימיזציה של מערכות טעינה אלחוטית דינמית בעלות יעילות העברת אנרגיה גבוהה המתורגמת לחיסכון ישיר של אנרגיה וכן לסוללות קטנות בהרבה. משמעות הדבר הינה חיסכון כספי עצום ופליטות פד"ח מופחתות משמעותית. אנו משוכנעים כי הממצאים המתוארים כאן יכולים לעזור לשפר מערכות טעינה דינמית אלחוטית קיימות, וליצור מערכות בטוחות, ירוקות, ויעילות יותר.

השפעת תצורות מגנטיות של סלילים על טעינה אלחוטית דינמית באפליקציות של רכבים חשמליים

תזת מחקר לתואר שני

מאת סהר בראלי

מנחים - פרופ' יוסף ישורון

- ד"ר שוקי וולפוס

המכון למוליכות על ולמדידות מגנטיות,

אוניברסיטת בר אילן, ישראל

26/09/2021